

Dear Author,

Here are the proofs of your article.

- You can submit your corrections **online**, via **e-mail** or by **fax**.
- For **online** submission please insert your corrections in the online correction form. Always indicate the line number to which the correction refers.
- You can also insert your corrections in the proof PDF and **email** the annotated PDF.
- For fax submission, please ensure that your corrections are clearly legible. Use a fine black pen and write the correction in the margin, not too close to the edge of the page.
- Remember to note the **journal title**, **article number**, and **your name** when sending your response via e-mail or fax.
- **Check** the metadata sheet to make sure that the header information, especially author names and the corresponding affiliations are correctly shown.
- **Check** the questions that may have arisen during copy editing and insert your answers/ corrections.
- **Check** that the text is complete and that all figures, tables and their legends are included. Also check the accuracy of special characters, equations, and electronic supplementary material if applicable. If necessary refer to the *Edited manuscript*.
- The publication of inaccurate data such as dosages and units can have serious consequences. Please take particular care that all such details are correct.
- Please **do not** make changes that involve only matters of style. We have generally introduced forms that follow the journal's style. Substantial changes in content, e.g., new results, corrected values, title and authorship are not allowed without the approval of the responsible editor. In such a case, please contact the Editorial Office and return his/her consent together with the proof.
- If we do not receive your corrections **within 48 hours**, we will send you a reminder.
- Your article will be published **Online First** approximately one week after receipt of your corrected proofs. This is the **official first publication** citable with the DOI. **Further changes are, therefore, not possible.**
- The **printed version** will follow in a forthcoming issue.

Please note

After online publication, subscribers (personal/institutional) to this journal will have access to the complete article via the DOI using the URL: [http://dx.doi.org/\[DOI\]](http://dx.doi.org/[DOI]).

If you would like to know when your article has been published online, take advantage of our free alert service. For registration and further information go to: <http://www.springerlink.com>.

Due to the electronic nature of the procedure, the manuscript and the original figures will only be returned to you on special request. When you return your corrections, please inform us if you would like to have these documents returned.

Metadata of the article that will be visualized in OnlineFirst

Please note: Images will appear in color online but will be printed in black and white.

ArticleTitle	Development of Carbon Materials for Energy and Environmental Applications	
Article Sub-Title		
Article CopyRight	Springer Science+Business Media, LLC (This will be the copyright line in the final PDF)	
Journal Name	Catalysis Surveys from Asia	
Corresponding Author	Family Name	Viswanathan
	Particle	
	Given Name	B.
	Suffix	
	Division	National Centre for Catalysis Research, Department of Chemistry
	Organization	Indian Institute of Technology, Madras
	Address	600036, Chennai, India
	Email	bvnathan@iitm.ac.in
Author	Family Name	Neel
	Particle	
	Given Name	P. Indra
	Suffix	
	Division	National Centre for Catalysis Research, Department of Chemistry
	Organization	Indian Institute of Technology, Madras
	Address	600036, Chennai, India
	Email	
Author	Family Name	Varadarajan
	Particle	
	Given Name	T. K.
	Suffix	
	Division	National Centre for Catalysis Research, Department of Chemistry
	Organization	Indian Institute of Technology, Madras
	Address	600036, Chennai, India
	Email	
Schedule	Received	
	Revised	
	Accepted	
Abstract	Methodologies for generating carbon materials from unusual natural sources like <i>Limonea acidissima</i> and <i>Calotropis gigantea</i> are reported. The carbon materials thus obtained have been characterized using a variety of tools. The possibility of modulating the textural properties of these materials has been examined. The carbon materials synthesized have been exploited for specific applications, such as support for noble metals for use in Direct Methanol Fuel Cells and as support for heteropoly acid for the production of gasoline additive. In addition, the utility of some of the activated carbon materials (from commercial sources) for the removal of sulphur from crude petroleum sources is also examined.	
Keywords (separated by '-')	Carbon materials - Carbon support - Direct methanol fuel cell - TAME - Adsorption of sulfur compounds	
Footnote Information		

Journal: 10563
Article: 9074



Author Query Form

**Please ensure you fill out your response to the queries raised below
and return this form along with your corrections**

Dear Author,

During the preparation of your manuscript for typesetting, some questions have arisen. These are listed below. Please check your typeset proof carefully and mark any corrections in the margin of the proof or compile them as a separate list. This form should then be returned with your marked proof/list of corrections to spr_corrections2@sps.co.in

Disk use

In some instances we may be unable to process the electronic file of your article and/or artwork. In that case we have, for efficiency reasons, proceeded by using the hard copy of your manuscript. If this is the case the reasons are indicated below:

- Disk damaged Incompatible file format LaTeX file for non-LaTeX journal
 Virus infected Discrepancies between electronic file and (peer-reviewed, therefore definitive) hard copy
 Other:

We have proceeded as follows:

- Manuscript scanned Manuscript keyed in Artwork scanned
 Files only partly used (parts processed differently:

Bibliography

If discrepancies were noted between the literature list and the text references, the following may apply:

- The references listed below were noted in the text but appear to be missing from your literature list. Please complete the list or remove the references from the text.
 Uncited references: This section comprises references that occur in the reference list but not in the body of the text. Please position each reference in the text or delete it. Any reference not dealt with will be retained in this section.

Queries and/or remarks

Section/paragraph	Details required	Author's response
	Please confirm the section headings are correctly identified.	
	Please check and confirm the family name and initials are correctly identified, in all references.	

1

2 Development of Carbon Materials for Energy and Environmental 3 Applications

4 B. Viswanathan · P. Indra Neel · T. K. Varadarajan

5

6 © Springer Science+Business Media, LLC 2009

7 **Abstract** Methodologies for generating carbon materials
8 from unusual natural sources like *Limonea acidissima* and
9 *Calotropis gigantea* are reported. The carbon materials
10 thus obtained have been characterized using a variety of
11 tools. The possibility of modulating the textural properties
12 of these materials has been examined. The carbon materials
13 synthesized have been exploited for specific applications,
14 such as support for noble metals for use in Direct Methanol
15 Fuel Cells and as support for heteropoly acid for the pro-
16 duction of gasoline additive. In addition, the utility of some
17 of the activated carbon materials (from commercial sour-
18 ces) for the removal of sulphur from crude petroleum
19 sources is also examined.

20
21 **Keywords** Carbon materials · Carbon support ·
22 Direct methanol fuel cell · TAME · Adsorption of
23 sulfur compounds

24 1 Introduction

25 Materials based on carbon have been evolving all the time.
26 In recent times these materials have given rise to a variety
27 of intriguing possibilities in terms of structure, morphol-
28 ogy, texture, properties and applications. However, one of
29 the challenging and desired aspects for carbon materials is
30 to find ways of producing these materials from alternate
31 (natural) sources and to tune the textural, structural and
32 surface properties in accordance with the application. This

A1 B. Viswanathan (✉) · P. I. Neel · T. K. Varadarajan
A2 National Centre for Catalysis Research, Department
A3 of Chemistry, Indian Institute of Technology, Madras,
A4 Chennai 600036, India
A5 e-mail: bvnathan@iitm.ac.in

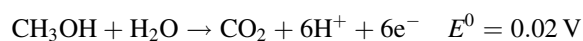
review reports the work carried out by the authors on the 33
preparation of carbon materials from plant sources and the 34
use of different carbons (natural and commercial) in 35
catalysis and adsorption. 36

2 Carbon Material from *Limonea acidissima* Shells 37 for Electrocatalytic Applications 38

Activated carbon materials from natural sources (ligno- 39
cellulosic materials) have been widely exploited for sorp- 40
tion and catalytic applications. Such materials have 41
remained unexplored for energy conversion device appli- 42
cations. Activated carbon material was synthesized from 43
Limonea acidissima (wood apple) shells using KOH as 44
activating agent. The carbon material (C_{WA}, Carbon from 45
wood apple shell) obtained was used as support for Pt. The 46
electrocatalyst Pt/C_{WA} was employed for the fabrication of 47
anode for the electrooxidation of MeOH [1]. 48

3 Fuel Cells as Clean Energy Sources 49

In a fuel cell, the chemical energy of the fuel is directly 50
converted to the electrical energy through a chemical 51
reaction [2]. Electric current can be generated by the direct 52
electrochemical oxidation of MeOH. The electrooxidation 53
reaction of methanol at the anode can be represented as 54
follows [3]: 55



The reaction of MeOH electrooxidation bears tech- 57
nological significance in the operation and exploitation of 58
Direct Methanol Fuel Cells. DMFCs hold promise as a clean 59
energy source for future transportation demands. Typical 60

Author Proof



stationary and mobile applications of fuel cells include electrification of residences, providing power to mobile phones, lap top computers and other portable electronic devices [4].

4 Challenges in the Development of Fuel Cell Anode Electrocatalysts

Platinum group metals (PGM's) are most widely used for electrode applications. There are two major problems associated with the development of DMFC. The first is poisoning of the electrode by CO [5]. Phosphoric acid fuel cells can withstand up to 2% CO in the fuel stream. But Proton exchange membrane fuel cells can only withstand ppm levels of CO. The second problem is the high cost of the catalyst restricting the rapid and wide spread commercialization of fuel cells. There are two approaches by which one can solve the above two problems. One approach is to find suitable alternatives (partial or complete) to the active component i.e., Pt and the second approach is to find suitable alternative to Vulcan XC 72 R carbon black which is the best carbon support material commercially used till date [6]. For example, Samant et al. [7] have generated a catalyst more active than 10 wt% Pt/Vulcan XC 72 R just by changing the support i.e., by replacing Vulcan XC 72 R with mesoporous carbon produced by a sol-gel method.

In general, high specific surface area carbon material is employed as support for Pt for fuel cell electrode applications. The carbon support facilitates the dispersion of the stable metal crystallites with favourable electronic and metal support interaction [8]. The carbon support influences the electrochemical properties and in turn the performance of Pt-based electrocatalysts. The nature of carbon material (oxygen surface functional groups, electronic conductivity, pore structure, morphology, electrochemically accessible surface area) determine the electrochemical performance of electrode catalysts. Electronic conductivity, surface area (electro active as well as BET), porosity, micro structure, macro morphology, corrosion resistance and cost are some of the important properties that determine the suitability of a carbon material for electrode applications.

Any breakthrough in the commercialization of DMFC's is possible only by significant improvements either in the replacement of *active Pt metal* or *the support carbon material*.

5 Carbon Material from *Limonea acidissima* Shell by KOH Activation

Limonea acidissima (Wood Apple) shells were conceived for the first time as a source for activated carbon. The fruit,



Fig. 1 Wood apple (*Limonea acidissima*) fruits

Limonea acidissima (Fig. 1.) is native to India and other Asian countries. *Limonea acidissima* is also called as *Feronia elephantum*, *Feronia limonia*, *Hesperethusa crenulata*, *Schinus limonia*, Wood apple, Elephant apple and Curd fruit. The shells of *Limonea acidissima* (wood apple) have features bearing close resemblance to that of coconut shells. Activated carbon from *Limonea acidissima* is produced by the chemical activation method using KOH as activating agent.

5.1 Method of Synthesis of Carbon Material

Typical method of synthesis of carbon material involves the soaking of a known amount (50 g) of dried shells of *Limonea acidissima* in 100 mL of 50 wt% KOH solution for 2 h. Excess KOH solution is then decanted. The shells soaked in KOH solution are then dried in an air oven at 150 °C followed by subjecting the same to thermochemical activation in a N₂ atmosphere at 800 °C for 2 h. The char thus obtained is subsequently treated with conc. HNO₃. The char to conc. HNO₃ ratio (wt/wt%) is 1:5.

5.2 Characterization of Carbon Material from *Limonea acidissima*

5.2.1 BET Sorptometry—Textural properties of Carbon Material

N₂ adsorption–desorption isotherms obtained for the activated carbon from *Limonea acidissima* are shown in Fig. 2. The corresponding pore size distribution curve (BJH) is also shown in the insert of the figure. The isotherm in Fig. 2 is of type I, characteristic of a microporous material. The pore size distribution reveals the pore dimensions to be less than 2 nm suggesting that the activated carbon material is microporous in nature.

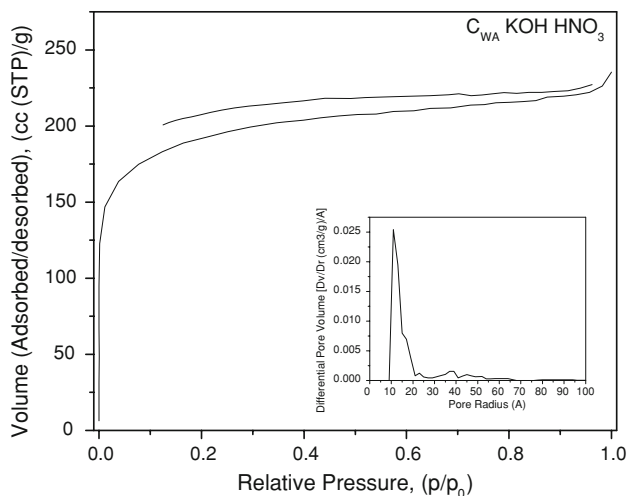


Fig. 2 N_2 adsorption-desorption isotherms of carbon materials prepared from *Limonea acidissima*; the corresponding pore size distribution of the activated carbon material is shown in the insert; $S_{\text{BET}} = 698 \text{ m}^2/\text{g}$; Pore volume (V_p) = $0.35 \text{ cm}^3/\text{g}$; and Mean pore diameter = 2.0 nm

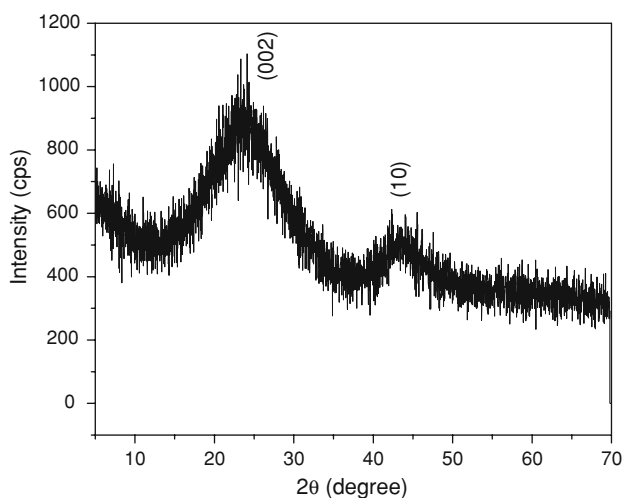


Fig. 3 XRD pattern of carbon material prepared from *Limonea acidissima* shells by KOH activation method

139 5.2.2 XRD Studies—Structural (Crystal) Details 140 of Carbon Materials

141 The X-ray diffraction pattern obtained for the activated
142 carbon material from *Limonea acidissima* shells is shown
143 in Fig. 3. Two broad diffraction peaks centered around 2θ
144 values of 24 and 43° which are, respectively, attributed to
145 the reflections from the (002) and (10) planes (the (hk) line
146 is because of intra layer scattering) of the carbon material.
147 The values of average crystallite sizes along the c-axis
148 (stacking axis) and the a-axis were determined using the
149 Debye–Scherrer equation. Shape factor, k , values of 0.89

and 1.84 were employed for the calculation of values of L_c 150
and L_a values respectively. The diffraction angles as well 151
as the value of full width at half maximum corresponding 152
to the diffraction planes of (002) and (10) were employed 153
for the calculation of values of L_c and L_a values respec- 154
tively. The values of L_c and L_a were found to be of the 155
order of 1.1 nm and 3.656 nm respectively. The values of 156
 L_c and L_a for typical graphitic carbon structure are 157
 0.0670 nm and 0.2461 nm respectively [9, 10]. The mag- 158
nitude of the values of L_c and L_a of the activated carbon 159
materials from *Limonea acidissima* (obtained by KOH 160
activation) indicate that the carbon material contained 161
roughly about 16 cell lengths along the c-direction and 162
nearly 15 cell lengths along the a-direction. 163

164 5.2.3 Confocal Raman Spectroscopic Studies— 165 Structural (Crystal, Order, Disorder, Defect) 166 Details of Carbon Materials

167 Details of structural disorder as well as the crystallographic
168 parameter of the activated carbon material produced by
169 KOH activation of the shells of *Limonea acidissima* were
170 obtained from the Confocal Raman spectrum shown in
171 Fig. 4. Two characteristic Raman peaks centered around
172 $1,348$ and $1,591 \text{ cm}^{-1}$ were observed in the confocal Raman
173 spectrum. These two bands were designated as D (disor-
174 dered) and G (graphitic) bands and were attributed to the A_{1g}
175 and E_{2g} Raman active C–C vibration modes with in the
176 graphitic layer. The Raman peaks at $1,348$ and $1,591 \text{ cm}^{-1}$
177 are called the first order Raman peaks. The other details
178 deduced from the Raman spectrum are: $R(I_D/I_G)$
179 = 1.408 ; $L_a = 4.4/R = 3.125 \text{ nm}$. This value is comparable
180 to the value of L_a deduced from XRD pattern (3.656 nm).

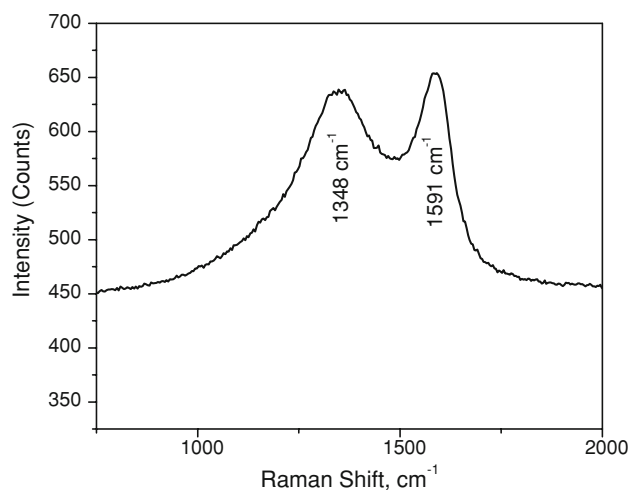


Fig. 4 Confocal Raman spectrum of activated carbon produced from *Limonea acidissima* by KOH activation

181 The Raman intensity ratio (the ratio of the integrated
182 intensities of the D and G bands) (I_D/I_G) is a measure of the
183 extent of disorder with in a carbon layer. The R value for
184 the activated carbon material from *Limonea acidissima* was
185 found to be 1.408 which is typical of disordered carbon
186 materials like glassy carbon. The slight variation ($\approx 5 \text{ \AA}$)
187 in the L_a value obtained between Confocal Raman spec-
188 trum and X-ray diffraction pattern is attributed to the $\pm 7\%$
189 error involved in the calculation of the integrated intensity
190 values under the D band and G band. Since line width from
191 XRD is more accurately determined compared to the
192 integrated intensity values under the D and G bands in the
193 confocal Raman spectrum, the L_a value obtained from wide
194 angle X-ray studies is more reliable.

195 5.2.4 Electron Paramagnetic Resonance Spectroscopic 196 Studies—Dangling Bond Concentration

197 The electron paramagnetic resonance (EPR) spectrum of
198 activated carbon from *Limonea acidissima* is shown in
199 Fig. 5. The EPR spectrum was recorded on a X-band EPR
200 spectrometer operating at a microwave frequency of
201 9.2 GHz at room temperature using diphenyl picryl
202 hydrazyl radical as the external reference. The g value of
203 the resonance signal for the activated carbon is 2.03095
204 which is close to the free electron g -value.

205 The origin of the EPR signal is attributed to the presence
206 of dangling bonds in the carbon structure. The concentra-
207 tion of unpaired spins was found to be 1.3×10^{18} spins/g
208 of the carbon material. The spin concentration value of
209 activated carbon from the stems of *Limonea acidissima*
210 (C_{WA}) is an order of magnitude lower than that of the spin
211 concentration values reported for commercial acetylene

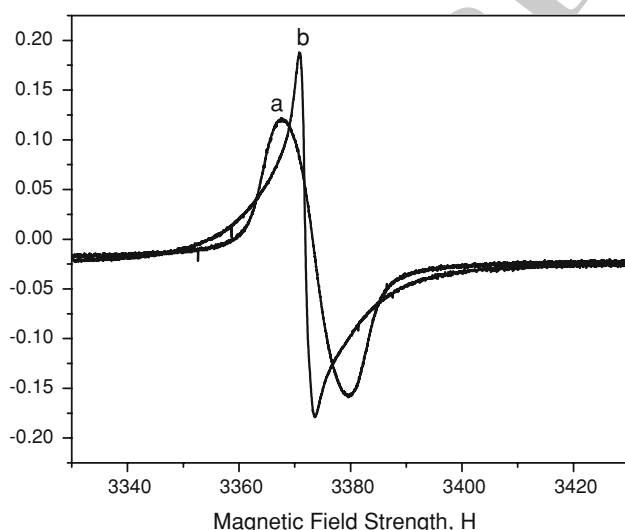


Fig. 5 EPR spectrum of activated carbon from a *Limonea acidissima* by KOH activation and b DPPH (reference)

212 based carbon (3.8×10^{19}) and graphon (1.1×10^{19}) [30].
213 The lower spin concentration in our sample is because of
214 the saturation of the dangling bonds with potassium,
215 formed during the carbothermal reduction of K_2CO_3 ,
216 resulting in the formation of surface C–K bonds which
217 subsequently transform (partially) to C–H bonds upon final
218 treatment with conc. HNO_3 . The formation of C–K type
219 bonds is also confirmed from the presence of 0.45 wt% K
220 in the activated carbon material even after treatment with
221 conc. HNO_3 (Fig. 6). The transformation is also confirmed
222 from the appearance of C–H bonds in the FT-IR spectrum
223 shown in Fig. 7.

224 5.2.5 Scanning Electron Microscopy and Energy 225 Dispersive X-ray Analysis—Morphology 226 and Elemental Composition

227 Details of the surface morphology as well as the elemental
228 composition of the activated carbon material were obtained
229 using High resolution scanning electron microscopy (HR
230 SEM, FEL, Model: Quanta 200) equipped with Energy
231 dispersive X-ray analysis facility. Scanning electron
232 microscope images are obtained at a magnification of
233 4,000 \times and 10,000 \times and at a scanning voltage of 30 kV.
234 A highly heterogeneous and rough surface with a contin-
235 uous porous net work is viewed on the surface of the
236 activated carbon produced from *Limonea acidissima*. The
237 porous network is clearly viewed at the higher magnifica-
238 tion (10,000 \times) (Fig. 6a, b).

239 The chemical composition of the activated carbon
240 material was determined using energy dispersive X-ray
241 analysis. A high carbon content of 74.84 wt% was found.
242 In spite of treatment with HNO_3 , 0.45 wt% K was inevi-
243 tably present in the activated carbon. The oxygen content
244 was found to be 24.7 wt% (19.83 atomic %).

245 5.2.6 FT-IR Spectroscopic Studies—Surface Functional 246 Groups

247 Fourier transform infrared (FT-IR) spectroscopy provides
248 evidence for the presence of specific functional groups on
249 the surface. The FT-IR spectrum of activated carbon from
250 *Limonea acidissima*, C_{WA} , was recorded on Shimadzu
251 spectrophotometer. The spectral range of analysis is 450–
252 4,000 cm^{-1} with a resolution of 4 cm^{-1} . The spectrum was
253 obtained in transmission mode at 20 scans. Pressed KBr
254 pellets were prepared by grinding 200 mg of carbon sam-
255 ples with 0.5 g of KBr. Several characteristic bands were
256 observed in the FT-IR spectrum shown in Fig. 7 and each
257 of the bands has been assigned to specific functional group
258 based on the assignments reported in literature.

259 Even though a cluster of functional groups are present
260 on the carbon surface, the prominent among them are: a

Fig. 6 SEM images and EDAX spectrum from the activated carbon material from *Limonea acidissima* using KOH activation; at a magnification of **a** 4,000 \times , **b** 10,000 \times , **c** selected region for elemental analysis and **d** energy dispersive X-ray analysis spectrum

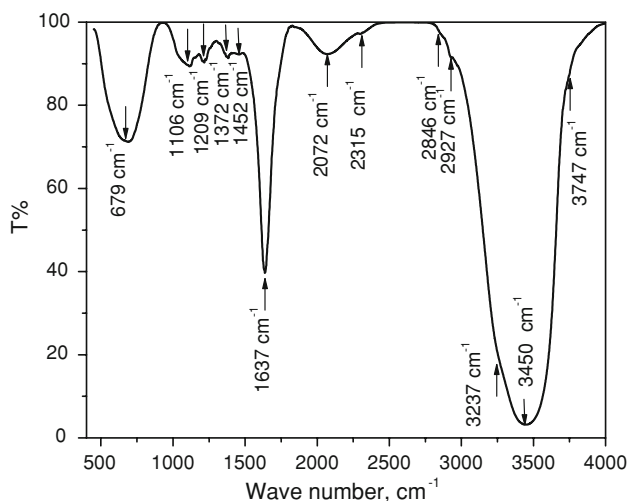
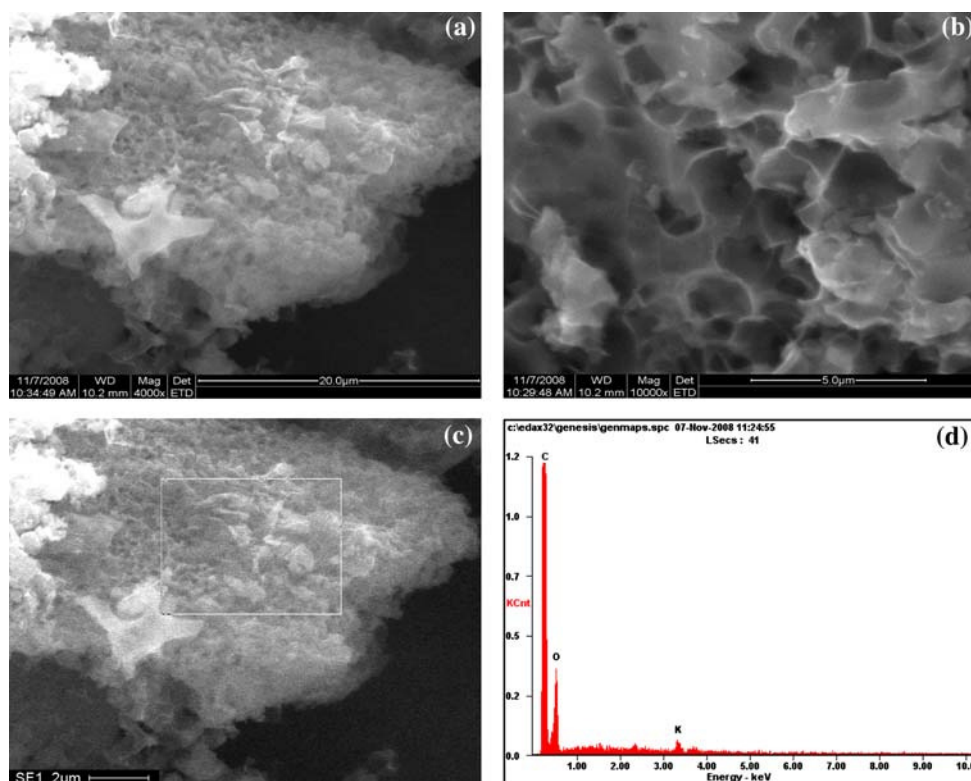


Fig. 7 FT-IR spectrum of activated carbon produced from *Limonea acidissima* shells using KOH activation

261 sharp and intense band centered around 1,637 $^{-1}$, which is
 262 attributed to the carbonyl (C=O) stretching vibration of
 263 quinone. The carbon surface is oxidized by treatment with
 264 conc. HNO₃ leading to the generation of such quinone type
 265 carbon functional groups, which bear significance in the
 266 redox chemistry of carbon materials. Such carbonyl func-
 267 tional groups are known to be pronounced in the case of
 268 oxidized carbon materials rather than the original parent

carbon material. In addition, a broad and intense band is 269
 observed in the range of 3,200–3,600 cm $^{-1}$, centered at 270
 3,450 cm $^{-1}$ attributable to the O–H stretching vibration of 271
 surface hydroxylic groups as well as to the adsorbed water. 272
 The asymmetry of this band (a shoulder at a lower wave 273
 number, 3,237 cm $^{-1}$) indicates the presence of strong 274
 hydrogen bonding interactions. 275

6 Fabrication of Anode Electrocatalyst for DMFC 276 Application with the Carbon Material Obtained 277 from *Limonea ascidissima* Shell 278

Lack of efficient and inexpensive electrocatalysts for 279
 MeOH oxidation is a challenge for the large scale utility of 280
 direct methanol fuel cells. The objective of this work is to 281
 design a cost effective and highly active electrocatalyst by 282
 developing new porous carbon material as support for Pt, 283
 as alternative to Vulcan XC 72 R. 284

6.1 Preparation of Pt/C Catalysts 285

Pt supported carbon catalysts have been prepared by 286
 impregnating hexachloroplatinic acid in carbon material 287
 followed by reduction of Pt (4+) to Pt (0) in hydrogen 288
 atmosphere at 450 °C for 2 h. Catalysts with different wt% 289
 loadings, namely, 5, 10 and 20 wt%, of active component 290

291 (Pt) on the carbon support (C_{WA}) were prepared by adding
 292 the requisite amounts of a H_2PtCl_6 solution to the carbon
 293 support (C_{WA}) and drying at 110 °C. A 20 wt% Pt/Vulcan
 294 XC 72 R prepared under identical conditions was
 295 employed as a reference for comparing the performance of
 296 C_{WA} carbon material relative to that of Vulcan XC 72 R
 297 carbon black.

298 6.1.1 XRD Analysis of Pt/C Catalysts

299 The X-ray diffractograms of 5, 10, and 20 wt% Pt on
 300 carbon material obtained from the shells of *Limonea aci-*
 301 *cidissima* (wood apple) are shown in Fig. 8. For comparison
 302 the XRD pattern of 20 wt% Pt/Vulcan XC 72 R is also
 303 shown in Fig. 8. Diffraction peaks characteristic of Pt
 304 metal with a face centered cubic lattice are observed and
 305 the peaks are all indexed as (111), (200), (220), (311) and
 306 (222) (JCPDS file No. 87-0647). The crystallite size of Pt
 307 calculated using Debye-Scherrer equation [11] and the
 308 lattice parameter values of Pt metal in the case of each of
 309 the catalysts (Pt/ C_{WA} and Pt/Vulcan XC 72 R) was cal-
 310 culated. The broad diffraction peak centered around a 2θ
 311 value of 24° corresponds to the (002) reflection of the
 312 carbon support with a turbostratic graphitic structure. The
 313 lattice constant value of ~0.39 nm correlates well with the
 314 FCC lattice of Pt metal supported on carbon materials
 315 [JCPDS file No. 87-0647]. The lattice constant value of Pt
 316 metal is (0.3923 nm) [12].

317 Reflection from the (220) plane of Pt metal was used for
 318 the calculation of the crystallite size as it is away from the
 319 region of the broad diffraction peak (from (002) plane) of

the carbon support. The crystallite size of Pt is found to be
 dependent on the Pt loading and also on the nature of the
 carbon support. With the same amount of Pt loading (20
 wt%), the crystallite size of Pt on carbon produced from
Limonea acidissima shell is smaller (10.4 nm) than on
 Vulcan XC 72 R (13.1 nm) indicating better dispersion of
 Pt on the C_{WA} support due to the enhanced surface oxygen
 functional groups as well as the higher value of specific
 surface area. Also, the Pt crystallite size was found to be
 the least (5 nm) in the case of 5 wt% Pt/ C_{WA} .

6.1.2 BET Sorptometric Studies—Textural Properties of the Pt/C Catalysts

The textural properties of the Pt/ C_{WA} catalysts were inves-
 tigated by BET sorptometry. At all loadings the Pt/ C_{WA}
 catalysts exhibited typical type I isotherms (not shown)
 characteristic of microporous solids. An important obser-
 vation was that the surface area and the volume of N_2
 (adsorbate) adsorbed decreased drastically as the wt% load-
 ing of Pt increased (5 wt% Pt/ C_{WA} [$S_{BET} = 505 \text{ m}^2/\text{g}$, $V_p =$
 $0.289 \text{ cm}^3/\text{g}$], 10 wt% Pt/ C_{WA} [$S_{BET} = 526 \text{ m}^2/\text{g}$, $V_p =$
 $0.288 \text{ cm}^3/\text{g}$] and 20 wt% Pt/ C_{WA} [$S_{BET} = 195 \text{ m}^2/\text{g}$,
 $V_p = 0.115 \text{ cm}^3/\text{g}$]. For comparison the textural properties
 of 20 wt% Pt/Vulcan XC 72 R catalyst are: ($S_{BET} = 123 \text{ m}^2/\text{g}$,
 $V_p = 0.294 \text{ cm}^3/\text{g}$).

7 Evaluation of Electrocatalytic Activity of Pt/C Catalysts

7.1 Electrooxidation of MeOH—Cyclic Voltammetry

Cyclic voltammetric studies were carried out on a BAS
 Epsilon potentiast using modified glassy carbon (Bioana-
 lytical system, USA) as the working electrode, Ag/AgCl
 (saturated KCl) as the reference electrode and a platinum
 foil (1.5 cm^2) as an auxiliary electrode. 0.5 M H_2SO_4 was
 employed as supporting electrolyte. The electrochemical
 measurements were carried out in a conventional three-
 electrode glass cell. The MeOH oxidation reaction was
 carried out with 1 M CH_3OH in acid medium.

The cyclic voltammograms recorded with electrodes
 fabricated using 5, 10 and 20 wt% Pt supported on carbon
 material C_{WA} are shown in Fig. 9. For comparison, the
 cyclic voltammetric response from the electrode fabricated
 with 20 wt% Pt supported on Vulcan XC 72 R is also
 shown in Fig. 9. The feature common to all the cyclic
 voltammograms is that one anodic peak is observed in the
 forward scan and another in the reverse scan. The anodic
 peak in the forward scan is attributed to oxidation of
 MeOH [13–18]. The anodic peak in the reverse scan is
 attributed to the removal of the incompletely oxidized

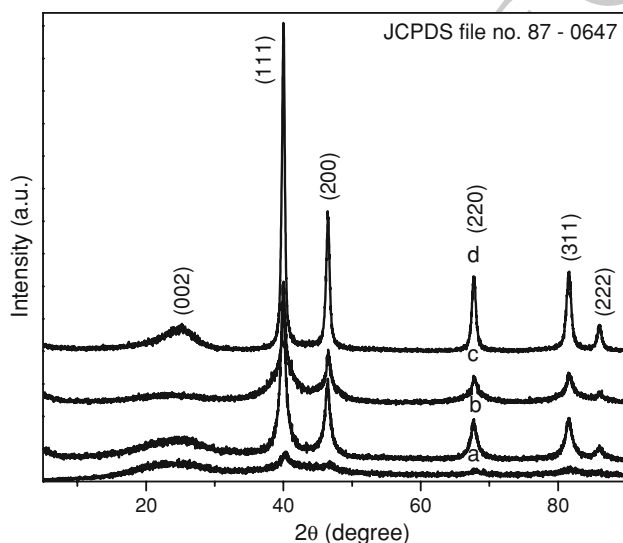


Fig. 8 X-ray diffraction patterns of *a* 5 wt% Pt/ C_{WA} (crystallite size ~5.0 nm) *b* 10 wt% Pt/ C_{WA} (crystallite size ~10.2 nm) *c* 20 wt% Pt/ C_{WA} (crystallite size ~10.4 nm) and *d* 20 wt% Pt/Vulcan XC 72 R (crystallite size ~13.1 nm)

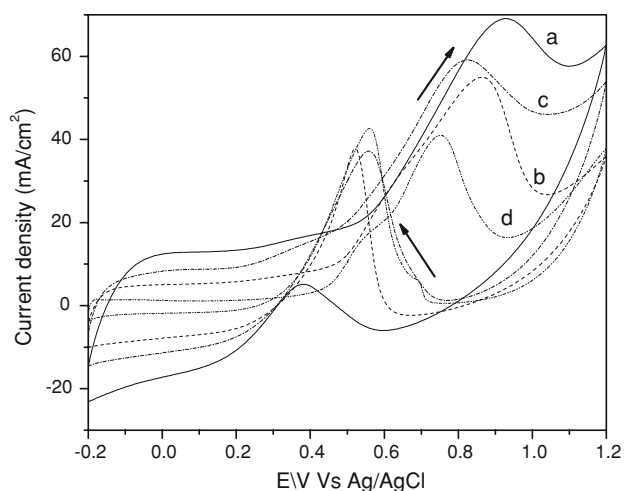


Fig. 9 Cyclic voltammetric response of *a* GC/C_{WA}—5 wt% Pt-Nafion electrode; *b* GC/C_{WA}—10 wt% Pt-Nafion electrode; *c* GC/C_{WA}—20 wt% Pt-Nafion electrode; and *d* GC/Vulcan XC 72 R—20 wt% Pt-Nafion electrode in 0.5 M H₂SO₄ and 1 M MeOH, at a scan rate of 25 mV/s between -0.2 and 1.2 V versus Ag/AgCl

367 carbonaceous species (mostly in the form of linearly bonded
368 Pt=C=O) formed in the forward scan [13].

369 The critical parameter that determines the usefulness of
370 an electrode is the onset potential. A less positive value of
371 the onset potential is preferred. A lower onset (less positive
372 potential) potential value implies the requirement of lower
373 energy of the MeOH oxidation reaction to take place [19].
374 The onset potential value is related to the breaking of the
375 C-H bond of MeOH which is the primary step involved in
376 the mechanism of electrooxidation of MeOH [20]. The onset
377 potential values for the electrooxidation of MeOH deduced
378 from the cyclic voltammograms obtained over different
379 electrodes, along with peak potential and current values
380 corresponding to the MeOH oxidation (anodic peak in the
381 forward sweep) as well as the oxidation of the intermediate
382 species formed during the oxidation of MeOH (anodic peak
383 in the reverse sweep) are summarized in Table 1. Zhaoling
384 Liu et al. [21] have reported the onset potential values of

0.27 and 0.28 V, respectively, on Pt/Vulcan XC 72 R and
Pt/CNT's for the electrooxidation of MeOH in 1 M H₂SO₄
and 2 M MeOH at a scan rate of 50 mV/s.

The onset potential being a little lower (0.21 V) than the
commercial vulcan carbon (0.25 V), 5 wt% Pt/C_{WA} showed
a higher current density which is an indication of higher
electrochemical catalytic activity. Such high current values
derivable from the modest wt% loadings of Pt is an indi-
cation of the effective utilization of Pt over the C_{WA} sup-
port. The improved performance of the electrocatalyst,
5 wt% Pt/C_{WA}, is attributed to the high electro catalytic
activity of the Pt nano crystallites (5.0 nm) finely dispersed
over the carbon support.

The ratio of the anodic peak current densities in the
forward (*i_f*) and reverse (*i_b*) scans too gives a measure of the
catalytic performance. A higher *i_f/i_b* ratio indicates superior
oxidation activity of methanol during the anodic scan and
less accumulation of carbonaceous species on the nano-
catalyst surface and thus an indication of better CO toler-
ance. The *i_f/i_b* value in the case of 5 wt% Pt/C_{WA} catalyst is
14.4 which is an order of magnitude higher than that of
either 20 wt% Pt/C_{WA} or 20 wt% Pt/Vulcan XC 72. The *i_f/i_b*
value of the electrocatalyst produced from commercial fuel
cell grade Vulcan XC 72 carbon was found to be 0.96. At all
the loadings of Pt, the electrodes fabricated using C_{WA}
carbon materials showed an *i_f/i_b* value greater than 0.96
(value obtained for Vulcan XC 72 R based catalyst). For
comparison, the *i_f/i_b* value for 20 wt% PtRu/C catalyst of
commercial Johnson Matthey sample is 1.33 [22].

7.2 MeOH Electrooxidation—Evaluation of Stability of the Electrode-Chronoamperometry

The long term stability of the fabricated electrodes was
evaluated by chronoamperometric studies carried out for a
duration of 3 h with the electrode being polarized at
+0.6 V versus Ag/AgCl in 0.5 M H₂SO₄ and 1 M MeOH.
The initial and final (after 3 h) current density values
derivable from the electrodes fabricated from 5, 10 and 20

Table 1 Effect of Pt loading and the nature of the carbon support on the electro catalytic activity of MeOH Electrooxidation of Pt/C_{WA} and Pt/Vulcan XC 72 R

S. no.	Electrode	Onset potential, V	<i>i_f/i_b</i>	Activity ^a			
				Forward sweep		Reverse sweep	
				<i>I</i> (mA/cm ²)	<i>E</i> (V)	<i>I</i> (mA/cm ²)	<i>E</i> (V)
1	GC/C _{WA} -5% Pt-Nafion	0.21	14.4	69.0	0.92	4.97	0.37
2	GC/C _{WA} -10% Pt-Nafion	0.18	1.45	55.0	0.86	37.6	0.52
3	GC/C _{WA} -20% Pt-Nafion	0.18	1.60	58.9	0.82	37.28	0.51
4	GC/Vulcan XC 72 R-20% Pt-Nafion	0.25	0.96	40.9	0.75	42.6	0.56

^a Activity evaluated in 0.5 M H₂SO₄ and 1 M MeOH, at a scan rate of 25 mV/s between -0.2 to 1.2 V versus Ag/AgCl

Table 2 Evaluation of the stability of C_{WA} based electrodes for the electrooxidation of MeOH in half cell mode

S. no.	Electrode	Activity ^a		% Decrease in activity after 3 h at +0.6 V
		Initial (I), [mAcm ⁻²]	Final (I), [mAcm ⁻²]	
1	GC/ C_{WA} -5% Pt-Nafion	25.2	19.1	24
2	GC/ C_{WA} -10% Pt-Nafion	29.7	19.0	36
3	GC/ C_{WA} -20% Pt-Nafion	36.1	3.7	89

^a Activity evaluated in 0.5 M H_2SO_4 and 1 M CH_3OH for 3 h with the electrode being polarized at +0.6 V versus Ag/AgCl

422 wt% Pt/ C_{WA} electrocatalysts are summarized in Table 2.
 423 The percentage decrease of the activity of the aforemen-
 424 tioned electrodes after 3 h is also shown in Table 2.
 425 Among the electrodes studied, the 20 wt% Pt/ C_{WA} catalyst
 426 based electrode showed least stability with a 89 percentage
 427 decrease of initial activity at the end of 3 h. In sharp
 428 contrast, as expected, the electrode fabricated using 5 wt%
 429 Pt/ C_{WA} possessing the smallest Pt crystallites (5.0 nm) as
 430 well as high i_f/i_b ratio showed highest stability. Only 24%
 431 loss in the initial activity is observed at the end of 3 h in the
 432 case of the GC/ C_{WA} —5% Pt-Nafion electrode. Thus, it is
 433 clear that the stability of the electrode is based on the
 434 smaller crystallite size of Pt as well as the high CO toler-
 435 ance (high i_f/i_b ratio value).

436 The activated carbon material produced from *Limonea*
 437 *acidissima* by KOH activation is a promising support for Pt
 438 for the electrooxidation of MeOH. The excellent perfor-
 439 mance of 5 wt% Pt/ C_{WA} is attributed to the increase in the
 440 extent of utilization of Pt metal. Thus the use of carbon
 441 material from *Limonea acidissima* as support for Pt offers
 442 the promise of effective utilization of Pt, high electrooxi-
 443 dation (MeOH) activity, high CO tolerance and long term
 444 stability. A strong correlation was found between the Pt
 445 crystallite size and the electrooxidation activity and stability
 446 of the carbon supported Pt catalysts.

447 8 Carbon Material from *Calotropis gigantea* 448 stems for Catalytic Applications

449 Microporous activated carbon with a large surface area and
 450 a narrow pore size distribution has been prepared from the
 451 dried stems of *Calotropis gigantea* [23]. *Calotropis*
 452 *gigantea* (Fig. 10) is a waste land weed native of India.
 453 Many activating agents, such as $ZnCl_2$, alkali and alkaline
 454 earth carbonates, organic acids and their salts have been
 455 used activation purposes. The characteristics (textural) of
 456 the prepared carbon materials were dependent on the
 457 activating agents used and the methodology used. A brief
 458 review of the preparation and the characteristics of the
 459 carbon materials prepared from the stems of *Calotropis*
 460 *gigantea* is now reported in the following section.



Fig. 10 Stems, leaves and flowers of *Calotropis gigantea*

9 Preparation of Activated Carbon Using $ZnCl_2$ as the Activating Agent

461
 462
 463 Activated carbon material was produced from *Calotropis*
 464 *gigantea* stems using $ZnCl_2$ as activating agent. Char (as
 465 synthesized) was obtained from *Calotropis gigantea* by
 466 heating the dried stems of the plant in a muffle furnace at
 467 300 °C [23]. The coal obtained was ground, sieved and
 468 treated with Conc. HCl to remove alkali and alkaline metal
 469 impurities. The char was further treated with a base
 470 (NaOH) to remove siliceous materials The process of
 471 activation with $ZnCl_2$ was carried out at 800 °C in N_2
 472 atmosphere for 8 h with varying amounts of activating
 473 agent to char (wt/wt%) ratios, namely, 1, 2, 3, 4 and 5.
 474 $ZnCl_2$ was added to the char in the solid state by
 475 mechanical grinding.

9.1 Characterization of Activated Carbon Produced from $ZnCl_2$ Activation

476
 477
 478 Textural and structural parameters and properties of the
 479 activated carbon materials were found to be influenced by
 480 the amount of the activating agent ($ZnCl_2$) as revealed from
 481 the Sorptometric, XRD and Confocal Raman studies.

Table 3 Effect of amount of activating agent (ZnCl_2) on the textural properties of carbon materials produced from *Calotropis gigantea*

S. no.	Sample	$\text{ZnCl}_2\text{:C}$ (wt/wt%)	S_{BET} (m^2/g)	V_{P} (cm^3/g)	Mean pore diameter ^a (nm)
1	Char	0	97	0.08	3.3
2	AC1	1	356	0.21	2.36
3	AC2	2	493	0.25	2.03
4	AC3	3	564	0.30	2.13
5	AC4	4	573	0.29	2.02
6	AC5	5	553	0.29	2.1

AC activated carbon

^a Mean pore diameter, $d = 4V/A$ (in nm), where V is the total pore volume and A is the specific surface area

482 9.1.1 BET Sorptometry—Textural Properties

483 Irrespective of the amount of the activating agent, all the
484 activated carbon materials presented type I adsorption
485 isotherms for N_2 adsorption at 77 K typical of microporous
486 materials. The specific surface area values, total pore vol-
487 ume as well as the average pore diameter details deduced
488 from the isotherms are summarized in Table 3. The specific
489 surface area values of the carbon materials produced
490 gradually increase (Table 3) with ZnCl_2 to char (wt/wt%)
491 ratio upto 4 and beyond which no increase in the S_{BET}
492 value is observed indicating that the optimum value of
493 $\text{ZnCl}_2\text{:Char}$ ratio is 4.

494 9.1.2 XRD Studies—Crystallographic Structure

495 The crystallographic parameters of the activated carbon
496 materials produced by ZnCl_2 activation of *Calotropis*
497 *gigantea* were obtained from X-ray diffraction studies.

498 Three typical broad diffraction peaks centered around 2θ
499 values of 25, 44 and 80° are visible in the activated carbons
500 generated with the activating agent to char impregnation
501 ratios of 1, 2, 3, 4 and 5. The two broad peaks centered
502 around the 2θ values of 25 and 44 are attributed (002) and
503 (10) diffraction peaks of turbostratic carbon structure [24].
504 The origin of the broad peak around 2θ value of 80° is not
505 yet clearly known. The (00 1) line is because of interlayer
506 scattering where as the (hk) line is because of intra layer
507 scattering. Thus the extent of graphitization is revealed by
508 the appearance of general (hkl) reflections [25–27]. The
509 occurrence of broad diffraction bands centered around 2θ
510 values of 25 and 44 indicates better layer alignment as well
511 as an increased regularity in the crystal structure [28].

Table 4 Effect of amount of activating agent (ZnCl_2) on the structural properties of carbon materials produced from *Calotropis gigantea*

S. no.	Sample	$\text{ZnCl}_2\text{:C}$ (wt/wt%)	d_{002} (nm)	L_{c} (nm)	L_{a} (nm)
1	AC1	1	0.356	1.04	3.94
2	AC2	2	0.356	1.02	3.50
3	AC3	3	0.353	1.03	3.96
4	AC4	4	0.356	0.91	3.72
5	AC5	5	0.350	0.94	3.80

AC activated carbon

The interlayer spacing values, d_{002} , and the crystallite
512 size values along the c (L_{c}) and a (L_{a}) axis of the turbostratic
513 graphitic carbon deduced from the X-ray diffracto-
514 grams are summarized in Table 4. Using the Scherrer
515 equation, the crystallite size along the c-axis, L_{c} and the
516 size of the large planes, L_{a} , were determined from the
517 diffraction peaks centered at 2θ values of 25 and 44° .
518

The interlayer spacing values, d_{002} , almost remained
519 unchanged with impregnation ratio of ZnCl_2 to char. The
520 interlayer spacing values, d_{002} , summarized in Table 4 are
521 in the range of 0.35–0.356 nm. These values are greater
522 than 0.335 nm, which is the typical value of the interlayer
523 spacing for pure graphitic carbon. L_{c} values for different
524 activated carbon materials, summarized in Table 4, are of
525 the order of 1 nm. A decreasing trend in the L_{c} value is
526 observed with an increase in the amount of the activating
527 agent. The L_{c} value is the smallest for the activated carbon
528 with the highest S_{BET} value. The L_{a} values varied in the
529 range of 3.5–3.96 nm. For typical graphitic carbon, the L_{c}
530 and L_{a} values are respectively 0.06708 and 0.2461 nm. The
531 magnitude of L_{c} and L_{a} values of the activated carbon
532 materials from *Calotropis gigantea* (obtained by ZnCl_2
533 activation) indicate that the carbon material was made up
534 of crystallites with dimensions of (on the average) about 15
535 cell lengths along the c-direction and about 14–16 cell
536 lengths along the a-direction.
537

9.1.3 Raman Scattering Studies—Order and Disorder
in Carbon Structure 538 539

The microstructural changes and the extent of crystallo-
540 graphic disorder (concentration of lattice defects in the
541 graphitic structure) in the activated carbon materials
542



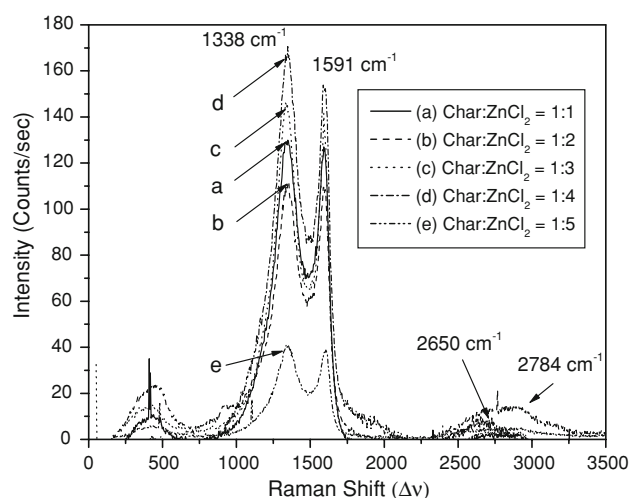


Fig. 11 Confocal Raman spectra of activated carbon materials prepared from *Calotropis gigantea* with a Char to ZnCl_2 ratio (wt/wt%) of a 1:1, b 1:2, c 1:3, d 1:4 and e 1:5

543 produced from *Calotropis gigantea* by employing ZnCl_2 as
 544 activating agent were analysed using confocal Raman
 545 Spectroscopic studies. The Raman spectra, shown in Fig. 11,
 546 resulting from activated carbon materials produced by
 547 varying the ratios of the activating agent (ZnCl_2) to the char
 548 (wt/wt%), namely, 1, 2, 3, 4 and 5, were recorded on a
 549 Confocal Raman instrument (CRM 200) using Ar ion laser
 550 (514.5 nm) as irradiation source.

551 Irrespective of the amount of the activating agent, all the
 552 carbon materials, showed both first order (1,200–1,600
 553 cm^{-1}) and second order (2,400–3,300 cm^{-1}) Raman lines.
 554 The information derived from the features of the first and
 555 second order Raman lines are important to access the
 556 structural order or disorder in the carbon structure and to find
 557 out whether it is amorphous or graphitic. First order Raman
 558 lines speak only about the structural order or disorder with in
 559 the carbon sheet or layer, ie, carbon plane along *a*-axis. They
 560 are silent about the stacking order or disorder in carbon
 561 structure. On the contrary, second order lines hold infor-
 562 mation about the structural (stacking) disorder along the
 563 crystallographic *c*-axis [29].

564 The two first order lines centered around 1,590 (D-band)
 565 and 1,348 (G-band) cm^{-1} are attributed to the graphitic and

disordered carbon structure. Here the term “graphitic” 566
 means carbon atoms which are three coordinated and are 567
 bound by sp^2 type bonding orbitals and has nothing to do 568
 with the stacking of layers along *c*-direction. The disorder 569
 in the carbon sheet may be because of the non-planar 570
 microstructure distortions or because of the disorganized 571
 regions near the crystal edges. Lattice defects such as edge 572
 dislocation and lattice vacancies too contribute to the band 573
 at 1,348 cm^{-1} . Important information extracted from the 574
 Raman spectra in Fig. 11 is summarized in Table 5. 575

The Raman intensity ratio (R) which is a measure of the 576
 extent of disorder (quantity of defects and vacancies and 577
 dislocations) is found to decrease initially upto the activating 578
 agent to char impregnation ratio of 3 beyond which it (R , 579
 disorder) increases. An inverse relation is observed between 580
 the value of R and the stack width L_a (crystallite size along 581
a-axis). The position of the D band (peak intensity position) and 582
 the relative intensity of the D band are found to be structure 583
 sensitive. An increase in the frequency value of the D band is 584
 correlated with a decrease in the crystallite size (L_a) and vice- 585
 versa. A strong correlation between the structural parameters 586
 deduced from XRD studies (Table 4) as well as Raman 587
 studies (Table 5) is observed as the two afore mentioned 588
 techniques are mutually complimentary to each other. Inter- 589
 estingly, the L_a values ($L_a = 44/R$ in Å) deduced from the 590
 relative intensity of the D band of the activated carbon 591
 materials correlates well with the L_a values obtained from 592
 XRD studies using the Scherrer equation (Table 4). But, it 593
 should be noted that the measurement of line width from the 594
 XRD is more accurate than the measurement of the integrated 595
 peak intensity values deduced from the Raman spectra. As a 596
 result, the L_a values derived from XRD are more reliable than 597
 those deduced from the Raman spectra. In addition, the 598
 integrated intensity values from Raman spectra are sensitive 599
 to the choice of the base line. As a result, the Raman intensity 600
 ratio's (R) shown in Table 5 are uncertain upto $\pm 7\%$. 601

9.1.4 Scanning Electron Microscopic Analysis—Details of Surface Morphology

The SEM image reveals that the carbon material is com- 604
 posed of sheets with well aligned uniform cylindrical pores 605
 of diameter (size) 2.4 μm (Fig. 12). 606

Table 5 Structural parameters (from Raman spectra) of the activated carbon materials from *Calotropis gigantea* activated with ZnCl_2

S. no.	Sample	ZnCl_2 : C (wt/wt%)	Peak intensity frequency, ν_x (cm^{-1})		$R = I_D/I_G$	L_a (nm) = 4.4/ R (from Raman)	L_a (nm) [from XRD]
			G band	D band			
1	AC1	1	1,591	1,348	1.40	3.14	3.94
2	AC2	2	1,591	1,355	1.42	3.09	3.50
3	AC3	3	1,591	1,331	1.33	3.30	3.96
4	AC4	4	1,587	1,348	1.48	2.97	3.72
5	AC5	5	1,606	1,348	1.53	2.87	3.80

AC activated carbon

10 Preparation of Carbon Materials from *Calotropis gigantea* Stems Using Alkali Metal Carbonates as Activating Agent

The maximum values of specific surface area and pore volume values from ZnCl_2 activation of the stems of *Calotropis gigantea* are only $573 \text{ m}^2/\text{g}$ and 0.29 cc/g . To attain further improvements in the textural parameters, the usefulness of alkali metal carbonates (Li_2CO_3 , Na_2CO_3 and K_2CO_3) as chemical activating agents was examined. The char obtained by heating the dried stems of plant in a muffle furnace at 300°C for 30 min was ground and sieved through a 200 mesh sieve to obtained fine carbon particles. It was next ground with the alkali carbonates in the desired proportion and activated at a temperature of 800°C for 8 h in N_2 temperature.

10.1 Characterization of Carbon Materials Produced Using Alkali Metal Carbonates as Activating Agent

10.1.1 XRD Studies—Phase Structure of Carbon Material

XRD patterns of carbon materials were recorded using Shimadzu XD-D1 X-ray diffractometer operated at a scan range of 0.05° with $\text{CuK}\alpha$ radiation ($\lambda = 1.5418 \text{ \AA}$) and a Ni filter. The XRD pattern of the char comprises two broad diffraction peaks centered at 2θ values of 10° and 22° . The broad diffraction peak at a 2θ value of 22° is characteristic of the presence of lignin component [30, 31].

Above a 2θ value of 27° several sharp and intense diffraction peaks are observed in the XRD profile from the char and they are a result of silica and other typical mineral matter present in the plant tissues which remain intimately bound with carbon material in the char. Treatment of the char with NaOH (10 wt% solution) followed by HCl treatment (conc.) removed significant amount of mineral matter. The sharp diffraction peaks characteristic of such mineral matter were completely absent in the char sample produced after NaOH and HCl treatment. Significant changes in the XRD profiles were observed upon activation of the char with K_2CO_3 . Upon activation, in addition to the retention of the inherent lignin structure, as evident from the retention of two broad peaks centered around 2θ values of 12° and 22° , a new diffraction peak originated at a 2θ value of 43.5° which is attributable to (10) diffraction of turbostratic carbon containing small hexagonal layer units of carbon. Similar observations are known in the literature [32, 33]. Beyond a char to K_2CO_3 ratio of 1:3, the intensity of the peak centered at 2θ value of 43.5° decreased steadily indicating the partial collapse of the turbostratic graphitic



Fig. 12 SEM image of activated carbon from *Calotropis gigantea* activated with ZnCl_2 (wt/wt% ratio of Char: ZnCl_2 is 1:3; from ref. [25])

structure leading to a disordered carbon structure with hexagonal carbon layers misoriented to one another.

10.1.2 BET Sorptometry—Textural Properties of Carbon Materials

The sorptometric analysis on the char (as-synthesized material from *Calotropis gigantea*) as well as the activated carbon materials were carried out on Sorptometric 1990 Carbo Erba sorptometer using N_2 as adsorbent at 77 K (-196°C). Prior to the analysis, the carbon samples were out gassed at 250°C for 12 h. Details of the textural properties of the carbon materials are presented in Table 6. The specific surface area (SSA) is found to be maximum ($1,296 \text{ m}^2/\text{g}$) at a K_2CO_3 to char ratio (wt/wt%) of 3 (Table 6). Thus, the optimum ratio of the activating agent to char is 3 (wt/wt%). At higher ratios, the SSA and the pore volume decreased.

The specific surface area of the activated carbon produced depends on the nature of the alkali cation, an increase in surface area of the carbon material is noticed with the radius of the cation of the activating agent (Table 7).

10.1.3 Effect of K_2CO_3 Activation on the Chemical Environment and the Concentration of Unpaired Electrons in Carbon from *Calotropis gigantea*

The EPR spectra of the char, char treated with base (NaOH) and acid (HCl) and the char activated with K_2CO_3 [char : $\text{K}_2\text{CO}_3 = 1:3$ (wt/wt)], shown in Fig. 13, were recorded on a Varian E-112, X band spectrometer at room temperature using DPPH (diphenyl picryl hydrazyl) as the

Table 6 Effect of amount of activating agent (K_2CO_3) on the specific surface area and pore volume values of carbon materials produced from *Calotropis gigantea*

S. no.	Sample	$K_2CO_3:C$ (wt/wt%)	Specific surface area (m^2/g)	Specific pore volume (cm^3/g)
1	Char (as synthesised)	0	97	0.08
2	Activated Carbon1	1	892	0.50
3	Activated Carbon2	2	1,083	0.59
4	Activated Carbon3	3	1,296	0.73
5	Activated Carbon4	4	765	0.45
6	Activated Carbon5	5	922	0.53

Table 7 Effect of nature of cation of the activating agent (char to carbonate ratio = 1:1 wt) on the textural properties of activated carbon

S. no.	Activating agent	Ionic radii of the cation (\AA) ^a	E^0 (V) ^{b,c}	Textural properties of carbon materials	
				Specific surface area (m^2/g)	Specific pore volume (cc/g)
1	Li_2CO_3	0.60	-3.0	480	0.263
2	Na_2CO_3	0.96	-2.7	811	0.395
3	K_2CO_3	1.33	-2.9	892	0.497

^{a,b} From ref. [34, p. 197]

^b $M + (aq) + e \rightleftharpoons M(s)$

^c The standard redox potential of activated carbon is +0.24 V [35]

external reference to evaluate the g factor value and the spin concentrations.

The g -factor values, peak to peak separation, ΔH in Gauss, and the spin concentration values were evaluated and are summarized in Table 8. The spin concentration values were determined by following the procedure described in reference [36].

Important details from the data derived from the EPR spectra shown in Fig. 13 and summarized in Table 8 are:

- the g factor values of the original char, char treated with base and acid as well as the char activated with K_2CO_3 are close to the g value of the free electron (2.002312) with in the error of our experiments (± 0.002). Manivannan et al. [37], Vilas Ganpat Pol et al. [25], Singer and Wagoner [38], Chauvert et al. [39], Zhuo et al. [40] have made similar observations in the case of carbon materials produced from a variety of precursors.
- the peak to peak separation was found to be higher in the case of the original char ($\Delta H = 11.0$ Gauss) compared to either the char treated with base and acid or the char activated with K_2CO_3 . Such a broadness in the EPR signal is attributed to the presence of SiO_2 in the original char which was confirmed from XRD analysis. The decrease in ΔH value upon treatment with base and acid indicates the removal of the silica. As early as 1968, Singer and Wagoner [38] have made similar observation of broadening of the EPR signal resulting from graphite because of the presence of

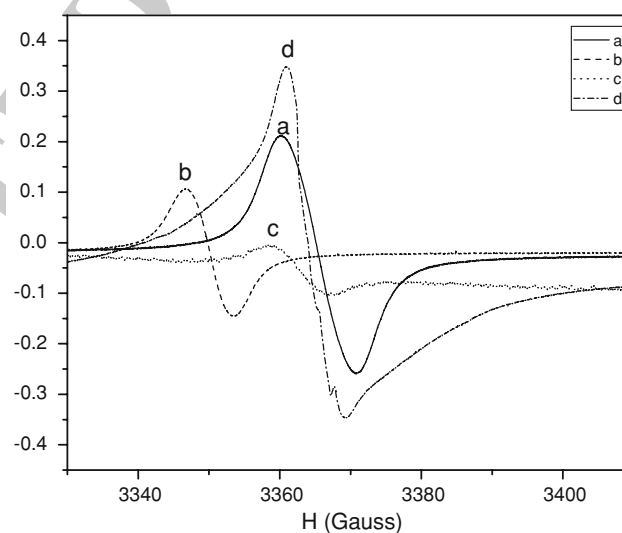


Fig. 13 EPR spectra of *a* char from *Calotropis gigantea*, *b* char treated with NaOH followed by HCl, *c* char activated with K_2CO_3 (char: K_2CO_3 (wt/wt%) = 1:3) and *d* DPPH

impurities like silica. Mrozowski has attributed the peak broadening to some changes in the structure of the carbon material [41]. Also from the data in Table 8, it is observed that upon activation with K_2CO_3 the ΔH value increased from 6.0 to 9.5 G indicating the presence of traces of K in the carbon material after activation leading to the slight broadening in the EPR signal.

Table 8 The g-factor, peak-to-peak separation (ΔH in Gauss) and concentration of unpaired electrons in the carbon materials produced from *Calotropis gigantea*

Carbon material	g-Value	ΔH (in Gauss) peak to peak separation	Spin concentration/g of carbon
Char (as synthesized)	2.00092	11.0	0.73×10^{19}
Char (base and acid treated)	1.99980	6.0	0.33×10^{19}
Char activated with K_2CO_3 (char: K_2CO_3 = 1:3, wt/wt%)	2.00058	9.5	0.15×10^{16}

Table 9 Chemical composition of carbon materials from *Calotropis gigantea*

Element (wt%)	Carbon materials from <i>Calotropis gigantea</i>		
	Char (as synthesized)	Base and acid treated (NaOH and HCl) treated	Activated with K_2CO_3 (Char: K_2CO_3 = 1:3)
Carbon	73.13	77.62	80.04
Hydrogen	2.61	2.63	3.50
Nitrogen	0.81	0.82	0.67
Sulphur	0.36	0.33	0.36
Total	76.91	81.40	84.57
Ash content	12.7	4.0	1.8
Oxygen ^a	10.39	14.6	13.63

^a By difference from the total amount of other constituents

719 3. The concentration of unpaired electrons in the char
720 was found to be of the order of $0.74 \times 10^{19}/g$. The
721 origin of such spins is attributed to the generation of
722 dangling bonds formed as a result of the extensive
723 devolatilization from the defragmentation of the
724 hemicellulose, cellulose and lignin structure during
725 the preparation of the char in the muffle furnace at
726 300 °C. Paramagnetic centers were found to be
727 associated with the dangling bonds formed during the
728 carbonization of carbon materials [42]. The spin
729 concentration of the graphon black and acetylene
730 black [43] were 1.1×10^{19} and 3.8 and 10^{19} spin/g,
731 respectively which are of the same order of magnitude
732 as that of the spin concentration value observed in the
733 case of the unactivated char shown in Table 8.

734 Upon treatment of the char with base and acid, the spin
735 concentration decreased from 0.74×10^{19} to 0.34×10^{19}
736 spin/g. Nearly a three orders of magnitude reduction in the
737 spin concentration is observed upon activation of char with
738 K_2CO_3 (0.15×10^{16} spins/g). Such a drastic decrease in
739 spin concentration upon activation with K_2CO_3 is because
740 of the saturation of the dangling bonds with K metal,
741 formed during the carbothermal reduction of K_2CO_3 ,
742 resulting in the formation of surface C–K bonds which
743 subsequently transform to C–H bonds upon final treatment
744 with conc. HCl. Such a transformation is also confirmed
745 from the increase in the hydrogen content (2.63–3.5 wt%)
746 of the carbon sample activated with K_2CO_3 and subse-
747 quently treated with conc. HCl (Table 7). Manivannan
748 et al. [37] have found the spin concentration values of
749 activated carbon materials, namely, GX203 (from coconut

Table 10 Influence of the chemical activator on the textural properties of carbon materials

S. no.	Chemical activator	S_{BET} (m ² /g)	Pore volume (V_p) [cm ³ /g]
1	Li ₂ CO ₃	478	0.26
2	Na ₂ CO ₃	811	0.40
3	K ₂ CO ₃	892	0.50
4	Ca(CO ₃) ₂	524	0.33
5	Ba(CO ₃) ₂	170	0.10
6	Zn(CO ₃) ₂	626	0.30
7	NaCl	400	0.20
8	NaBr	319	0.16
9	KBr	275	0.10
10	NaI	58	0.04
11	CaO	521	0.25
12	Ca(OH) ₂	189	0.11
13	CaCl ₂	156	0.09
14	Ba(OH) ₂	152	0.08
15	Al(NO ₃) ₃	253	0.19
16	Urea	439	0.21
17	Sodium acetate	548	0.26
18	Sodium oxalate	707	0.33
19	Sodium potassium tartarate	394	0.20
20	Sodium citrate	419	0.20
21	Sodium tartarate	394	0.20
22	Citric acid	127	0.07
23	Tartaric acid	42	0.04
24	Oxalic acid	317	0.14

The activation conditions are: carbon precursor:chemical activator (wt/wt%) ratio of 1:1, activation temperature of 800 °C, duration of activation is for 2 h



750 shell precursor), P1400 (from wood precursor) and Med50
751 (from coconut shell precursor) to be 1.8×10^{17} , $5.8 \times$
752 10^{17} and 1.8×10^{16} spins/g, respectively.

753 10.1.4 Elemental Analysis—Chemical Constitution 754 of Carbon Materials

755 The elemental analysis of the char, char treated with NaOH
756 followed by HCl and char activated with K_2CO_3
757 (char: K_2CO_3 (wt/wt%) = 1:3) was carried out in a CHNS/
758 O analyzer (Perkin Elmer Instrument, Series II) and the
759 results are presented in Table 9.

760 A simple treatment of the char with NaOH (10 wt%
761 solution) and HCl in succession has improved the carbon
762 content (wt%) from 73.13 to 77.62 which is attributed to
763 the elimination of mineral matter. Activation with
764 K_2CO_3 has further increased the carbon content from
765 77.62 to 80.04% and also the oxygen content decreased
766 from 14.6 to 13.6% as expected. The increase in
767 hydrogen (2.63–3.5 wt%) upon activation with K_2CO_3 is
768 not because of activation step (reaction), but because of
769 the subsequent treatment of the activated carbon com-
770 posite (carbon material with the decomposed products of
771 activated carbon, mainly K) with HCl and further
772 washing with water. During the K_2CO_3 activation pro-
773 cess surface specie such as C–O–K are formed, which
774 upon treatment with HCl and subsequent washing with
775 water get transformed to C–O–H groups contributing to
776 an increase in the hydrogen content in the case of acti-
777 vated carbon sample relative either the original char or
778 the base and acid treated char.

779 11 Effect of the Nature of Activating Reagent 780 on the Textural Properties of Activated 781 Carbon Materials

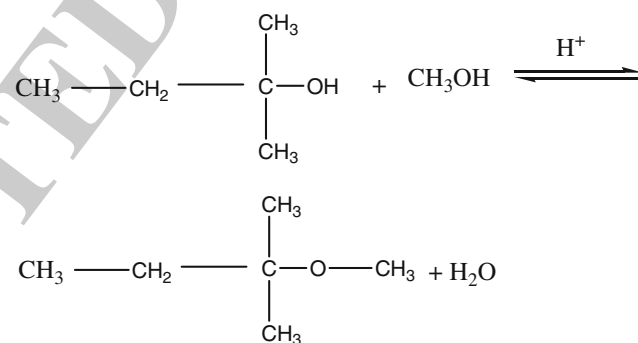
782 The potential of various chemical compounds in tuning the
783 textural properties of carbon materials is summarized in
784 Table 10. All the carbon materials exhibited Type I iso-
785 therms characteristic of microporous materials. It is
786 observed that alkali salts of some carboxylic acids are as
787 effective as alkali metal carbonates in improving the tex-
788 tural properties of carbon materials.

789 12 Catalytic Application of Carbon Materials 790 for the Synthesis of Tert-Amyl 791 Methyl Ether (TAME)

792 In the condensation reaction of tert-amyl alcohol (TAA)
793 and methanol to form TAME, water is formed as a

794 byproduct. The catalyst needs to be hydrophobic to resist
795 the leaching of the active component. Carbon materials
796 are sufficiently hydrophobic owing to the presence of
797 graphite like chemical properties and can form an integral
798 component of the catalyst. Acid function is the catalytic
799 component needed to drive the etherification reaction.
800 Heteropoly acids, particularly, dodeca tungstophosphoric
801 (HPW) acid is a strong super acid with a H_0 value of
802 -13.4 (more acidic than 100% sulphuric acid, $H_0 =$
803 -11.94).

804 Four different carbon materials, namely, activated
805 carbon from *Calotropis gigantea* (ACCG from K_2CO_3
806 activation), Black Pearl, Vulcan XC 72 R and CDX 975
807 with varying textural properties (Table 11) were
808 employed as support material for HPW to evaluate the
809 effect of the nature of carbon support on the activity of
810 the supported solid acid catalyst. The HPW/C catalysts
811 were prepared by impregnation-drying method using
812 aqueous solutions of HPW. The carbon material and the
813 HPW solutions were stirred at room temperature for 6 h
814 followed by drying at $80^\circ C$ in a water bath to obtain 10
815 wt% HPW/C.



816 The catalytic activity of carbon supported heteropoly
817 acids was investigated in the vapour phase synthesis of
818 TAME as a test reaction. The reaction was carried out in a
819 down flow fixed bed reactor at atmospheric pressure at a
820 temperature of 373 K. The liquid feed containing tert-amyl
821 alcohol (TAA) and methanol (in the mole ratio of 1:10)
822 was fed onto the catalyst bed through a peristaltic pump
823 (Miclins, SPO1) at a flow rate of 10 mL/h. N_2 was used as
824 a carrier gas (flow rate, 30 mL/min). In a typical run, 0.5 g
825 of the catalyst was charged in the reactor. The catalyst was
826 stacked between glass beads and ceramic wool. The reactor
827 was maintained under isothermal conditions during all
828 runs. The reaction products were condensed at the bottom
829 of the reactor and analyzed for the chemical composition
830 using a gas chromatograph equipped with an OV 101
831 (packed) column and a FID detector.

Table 11 Textural properties of the carbon materials and their catalytic activity after loading HPW (10 wt%) in the synthesis of TAME

Carbon material	S_{BET} (m^2/g)	Density (g/cc)	V_p (cc/g)	Conversion ($\text{wt}\%$) ^a	Selectivity (%)	
					Olefins	TAME
CDX 975	215	0.23	0.28	75	35	65
Vulcan XC 72 R	224	0.33	0.46	54	13	87
Black Pearl 2000	1,012	0.15	1.15	7	47	53
Activated carbon— <i>Calotropis gigantea</i> (ACCG)	1,291	0.28	0.73	32	37	73

Reaction conditions: time on stream = 3 h; tert-amyl alcohol/methanol (mole) = 1:5; flow rate of the feed = 10 mL/h; flow rate of the carrier gas = 30 mL/min; amount of catalyst = 0.5 g

^a Olefins: 2-methyl-2-butene (2MB2), 2-methyl-1-butene (2MB1)

832 The condensation reaction between tert-amyl alcohol
833 and methanol over HPW/C catalysts was monitored for 3 h
834 (Fig. 14). Reaction products were collected and analyzed
835 by GC at intervals of 30 min. The catalytic activity was
836 evaluated by monitoring the conversion of TAA with time.
837 In situ generation of iso-amylenes (2-methyl-1-butane,
838 2MB1, and 2-methyl-2-butene, 2MB2) was observed dur-
839 ing the course of the reaction. The formation of iso-
840 amylenes is a result of the dehydration of the tert-amyl
841 alcohol. The iso-amylenes formed subsequently react with
842 MeOH to form TAME. Details of conversion (wt%) of
843 TAA and selectivity towards olefins and TAME over dif-
844 ferent HPW/C catalyst are summarized in Table 11. The
845 results reveal that the activity and selectivity are not
846 apparently related to the surface areas of the carbon sup-
847 ports. Activity for the etherification could be related to
848 many factors, such as the dispersion of HPW, the distribu-
849 tion of HPW in the pores, the accessibility of the active
850 sites (through diffusion) to the reactants and the presence/
851 absence of poisons on the surface of the support. All the

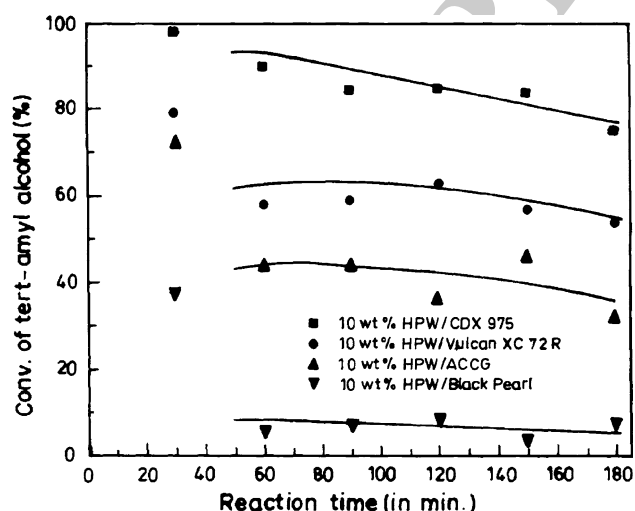


Fig. 14 Plot of conversion of TAA (wt%) versus reaction time (in minutes)

852 catalysts tend to deactivate slowly with duration of run,
853 the more active catalyst (CDX 975) deactivating faster than
854 the other (Fig. 14).

13 Carbon Materials (as Adsorbents) for Adsorptive Desulfurization

13.1 Studies on Neat Carbon Samples

858 Removal of organo-sulphur compounds from diesel is an
859 issue of interest from scientific, social, economic and
860 environmental view points. Production of clean fuel is the
861 goal of petroleum refining industry. The reduction of S
862 below certain levels in diesel fuels becomes difficult due to
863 the presence of sterically hindered S-compounds (such as
864 the 4,6-dialkydibenzothiophenes) that are difficult to
865 desulfurize over conventional supported mixed sulfide
866 catalysts. Hence, newer technologies based on novel routes
867 like adsorption, oxidation and chelation are being devel-
868 oped to remove these refractory S-compounds. We now
869 summarize in the following section our work on the use of
870 carbon materials for the adsorptive desulfurization of a
871 medium S-containing straight run diesel fraction with a S
872 content of 737 ppm, from Cauvery Basin Refinery (CBR),
873 India.

874 The physicochemical properties of the CBR diesel are
875 summarized in Table 12. Several commercially available
876 activated carbon materials of varying physical and chem-
877 ical properties were tested as adsorbents for the removal of
878 organo sulphur compounds from CBR diesel. The carbon
879 materials used were adsorbent carbon (A) from Adsorbent
880 Carbons Pvt. Ltd., India. Calgon carbon (B) from Calgon
881 Carbon (Tianjin) Co. Ltd., Activated carbons, IG 18 × 40,
882 IG 12 × 40 and IG 8 × 30 from Indo-German Carbon
883 Ltd., India and the Activated carbons, AC 4 × 8, AC
884 6 × 12, AC 12 × 30 from Active Carbon Pvt. Ltd., India.

885 In a typical adsorption experiment, a glass column of
886 length 50 cm and internal diameter 1.5 cm was packed

Table 12 Properties of SR diesel from CBR distillation unit used in the studies

Property	Value
Total sulphur content (in ppm)	737
Flash point (°C)	93
Aniline point (°C)	81
Viscosity (at 40°C in cSt)	4.04
Pour point (°C)	+6
Density (g/cc)	0.8553
Diesel index	60
Cetane index	53

887 with 5.0 g of carbon sorbent with glass beads on either
 888 side. Diesel was fed on top of the sorbent bed. The first
 889 20 mL product collected at the out let was analyzed for
 890 S. From the S content remaining in the product and sub-
 891 tracting the same from the S content in the feed diesel
 892 (737 ppm), the S removed by the carbon was obtained. The
 893 S content in the product was analyzed by using an Oxford
 894 XRF analyzer. The feed and the product diesel were also
 895 analyzed (in some experiments) for individual sulphur
 896 compounds using a GC-PFPD (Gas Chromatography–
 897 Pulsed Flame Photometric Detector).

898 Different commercially available activated carbons,
 899 namely, IG 18 × 40, IG 12 × 10, IG 8 × 30, AC 4 × 8,
 900 AC 6 × 12, AC 12 × 30, calgon carbon as received and
 901 adsorbent carbon as received were used as adsorbents for S
 902 containing compounds present in SR diesel. The results
 903 obtained on the studies with the afore mentioned adsor-
 904 bents are given in Table 13. The amount of S removed (in
 905 ppm) from 20 mL diesel by 5.0 g of sorbent is shown in
 906 extreme right column of Table 13. Among the eight car-
 907 bons studied adsorbent carbon as received and calgon
 908 carbon as received were superior to the others for the
 909 adsorption of S-compounds in diesel. Hence, adsorbent

Table 13 S removal capacity of different commercial activated carbon materials

Activated carbon as sorbent	20 mL-diesel treated/g of adsorbent ^a	S removed (ppm)
IG 18 × 40	4	134
IG 12 × 10	4	81
IG 8 × 30	4	76
AC 4 × 8	4	12
AC 6 × 12	4	73
AC 12 × 30	4	92
Calgon carbon as received	4	181
Adsorbent carbon	4	229

^a A 20 mL initial product collected from the column packed with 5.0 g activated carbon and analyzed for S

carbon (A) and calgon carbon (B) were selected for sub-
 sequent studies.

13.2 Studies on Activated Carbon Samples [Adsorbent Carbon (A) and Calgon Carbon (B)]

13.2.1 Activation with Conc. HNO₃

HNO₃ treatment changes the surface chemistry of carbon materials. Such oxidative treatment results in the formation of oxygen containing surface functional groups (carbonyl and carboxyl). The presence of such surface functional groups, in most cases, enhances the adsorption capacity of carbon materials [44, 45]. Two commercial activated carbon materials, namely, the adsorbent carbon (A) and the calgon carbon (B) were treated with conc. HNO₃. The wt/wt% ratio of carbon to conc. HNO₃ was 1:5. The oxidative treatment of carbon with conc. HNO₃ was carried out at 60 °C for 2 h under refluxing conditions in a 2-L RB flask. The contents were then cooled to room temperature, washed with water and dried at 110 °C for 2 h.

13.2.2 Activation Under Ar Atmosphere

Ar activation involved the thermal activation of nitric acid treated carbon materials A and B at a temperature of 800 °C under Ar atmosphere for 2 h in a quartz tube. The carbon samples after activation were termed as nitric acid treated Ar activated carbon materials.

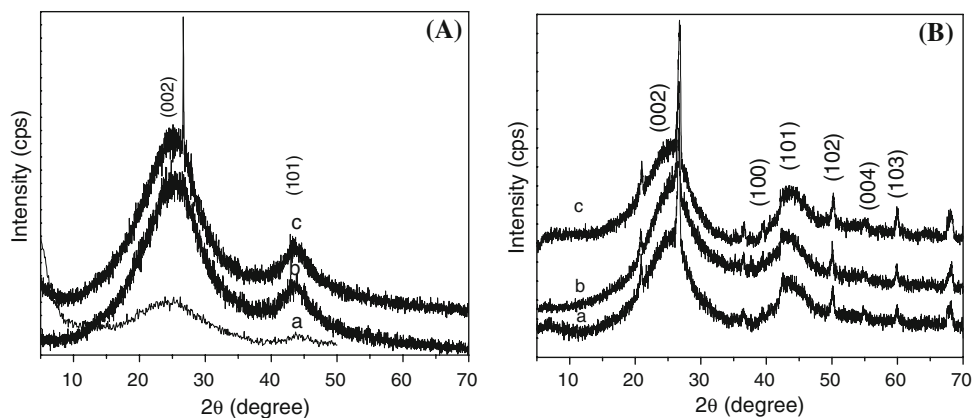
13.3 Characterization of Adsorbents for Desulphurization Application

13.3.1 XRD Analysis

X-ray diffraction patterns of adsorbent carbon as received, adsorbent carbon treated with conc. HNO₃ and adsorbent carbon treated with HNO₃ followed by subsequent activation in Ar atmosphere are shown in Figs. 15A(a–c), respectively. Two broad diffraction peaks centered at 2θ values of 25.4 and 43.4 are observed in all the patterns. These peaks can be indexed, respectively, to (002) and (101) planes of crystalline hexagonal graphite lattice [(JCPDS-41-1487), 46].

The phase structure of adsorbent carbon remained unaltered upon nitric acid treatment [Fig. 15A(a, b)]. But in the case of adsorbent carbon treated with nitric acid followed by activation in Ar atmosphere an additional intense and narrow diffraction peak is seen at $2\theta = 26.7$ [Fig. 15A(c)]. This is attributed to (002) reflection from highly crystalline graphitic carbon [47]. Nitric acid treated Ar activated adsorbent carbon [Fig. 15A(c)] is more crystalline than either adsorbent carbon as received or adsorbent carbon

Fig. 15 XRD patterns of **A:** *a* adsorbent carbon as received, *b* adsorbent carbon treated with HNO₃ and *c* adsorbent carbon treated with HNO₃ and activated with Ar; **B:** *a* calgon carbon as received, *b* calgon carbon treated with HNO₃ and *c* calgon carbon treated with HNO₃ followed by Ar activation



955 treated with nitric acid alone. Thus Ar activation improved
956 the crystallinity of nitric acid treated adsorbent carbon.

957 X-ray diffraction patterns of calgon carbon as received,
958 calgon carbon treated with HNO₃ and calgon carbon treated
959 with HNO₃ followed by Ar activation are shown in
960 Fig. 15B(a–c), respectively. The diffraction peaks arising
961 from each of these carbon samples were indexed and are
962 typical of graphitic carbon structure [47]. Neither HNO₃
963 treatment [Fig. 15B(b)] nor HNO₃ treatment with sub-
964 sequent Ar activation [Fig. 15B(c)] significantly altered the
965 structure of the original calgon carbon sample
966 [Fig. 15B(a)]. Thus, neither HNO₃ treatment nor Ar acti-
967 vation has much influence on the phase structure of calgon
968 carbon.

969 There is a marked difference in the structural order
970 between adsorbent carbon and calgon carbon. No diffrac-
971 tion peaks resulted from adsorbent carbon or its modified
972 forms beyond $2\theta = 50^\circ$ (Fig. 15A) in sharp contrast to the
973 characteristic diffraction peaks resulting from Calgon and
974 modified calgon carbon above $2\theta = 50^\circ$ (Fig. 15B). Thus,
975 calgon carbon appears to be structurally more ordered than
976 adsorbent carbon.

977 13.3.2 BET Sorptometric Studies

978 The N₂ adsorption-desorption isotherms (not shown) of the
979 different treated adsorbent carbons were typically of the
980 type I (characteristic of microporous materials) while those
981 of the Calgon based samples were slightly different in that
982 some multilayer adsorption was also noticed suggesting the
983 presence of larger (meso) pores. The surface area and pore
984 volumes of the different samples are presented in Table 14.

985 13.3.3 FT-IR Studies

986 The FT-IR spectra of adsorbent carbon and calgon carbon,
987 as received, treated with HNO₃ and treated with HNO₃
988 followed by Ar activation are presented in Fig. 16A, B.

Table 14 Surface area and pores volumes of adsorbent carbon, calgon carbon and their modified forms

Carbon	Specific surface area (m ² /g)	Total pore volume (cm ³ /g)
Adsorbent carbon as received	950	0.451
Adsorbent carbon treated with Conc. HNO ₃	882	0.398
Adsorbent carbon treated with Conc. HNO ₃ followed by Ar activation	1,048	0.523
Calgon carbon as received	1,014	0.587
Calgon carbon treated with Conc. HNO ₃	649	0.387
Calgon carbon treated with Conc. HNO ₃ followed by Ar activation	996	0.598

989 The main distinguishing feature observed in the Acti-
990 vated carbon samples after nitric acid treatment is the
991 generation of a shoulder at 1,749 cm⁻¹ [Fig. 16A(b)]
992 attributed to the stretching vibration of C=O bond (alde-
993 hydies, ketones, lactones or carboxyl groups). This shoulder
994 at 1,749 cm⁻¹ becomes intense and develops into a sharp
995 peak upon activation in Ar atmosphere [Fig. 16A(c); 48,
996 49]. But for this difference all the three samples showed
997 similar but rich surface chemistry with a variety of oxygen
998 containing functional groups. A number of functional
999 groups are common to adsorbent carbon and its modified
1000 forms [Fig. 16A(a–c)]. These are: a sharp band at
1001 3,738 cm⁻¹ is ascribed to isolated OH groups, a broad,
1002 intense band in the range of 3,200–3,600 cm⁻¹ with a
1003 maximum at about 3,440 cm⁻¹ assigned to the O–H
1004 stretching mode of hydroxyl groups and adsorbed water
1005 [50], two sharp, narrow and intense bands at 2,922 and
1006 2,855 cm⁻¹ as a result of, respectively, the asymmetric and
1007 symmetric C–H stretching vibrations of the methylene
1008 group [51–53], a sharp intense peak at 1,640 cm⁻¹ attrib-
1009 uted to the carbonyl groups in quinone, broad bands
1010 observed in the range of 1,300–1,000 cm⁻¹ attributed to

Fig. 16 FT-IR spectra of **A:** *a* adsorbent carbon as received, *b* adsorbent carbon treated with HNO₃ and *c* adsorbent carbon treated with HNO₃ and activated with Ar; **B:** *a* calgon carbon as received, *b* calgon carbon treated with HNO₃ and *c* calgon carbon treated with HNO₃ followed by Ar activation

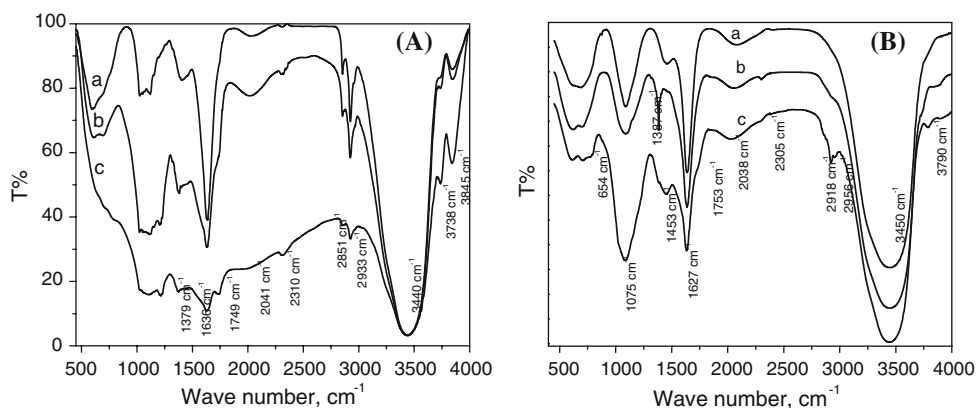


Table 15 S sorption capacity of the different carbon samples

Carbon	S removed ^a (in ppm)
Adsorbent carbon as received	410
Adsorbent carbon treated with HNO ₃	577
Adsorbent carbon treated with HNO ₃ followed by Ar activation	586
Calgon carbon as received	451
Calgon carbon treated with HNO ₃	488
Calgon carbon treated with HNO ₃ followed by Ar activation	619

^a S removed from the first 20 mL diesel after passing through the sorbent bed; S content in the diesel feed—737 ppm; Carbon loading: 15 g

Table 16 Type and amount of the S compounds in the feed and the product diesel (after passing through the carbon bed) as analyzed by GC-PFPD [55]

Sulphur species	S content (in ppm)		
	CBR diesel (feed)	Adsorbent carbon HNO ₃ followed by Ar treatment, 15.0 g	Calgon carbon, HNO ₃ followed by Ar treatment, 15.0 g
C ₁ BT	4.6	Nil	Nil
C ₂ BT	119.6	Nil	Nil
C ₃ BT	137.5	75.2	67.2
C ₃ ⁺ BT	79.6	68.9	47.4
DBT	91.5	2.6	1.3
C ₁ DBT	157.7	Nil	Nil
C ₂ DBT	116.7	Nil	Nil
C ₃ DBT	29.5	4.3	2.1
Total S	737	151	118

^a C₁, C₂, C₃, C₃⁺ BT and DBT—mono, di, tri and multi alkyl substituted benzothiophene and dibenzothiophenes

1011 C–O stretching in acids, alcohols, phenols, ethers and
1012 esters and lastly, broad bands in the range of 600–
1013 800 cm⁻¹ as a result of the out of plane deformation mode
1014 of C–H in various substituted benzene rings [50, 51].

In the case of the calgon carbon samples (Fig. 16B), activation with conc. HNO₃ creates new bands at 3,790, 2,305 and 1,387 cm⁻¹ attributable to isolated O–H groups, ketone surface groups [54] and the in-plane bending vibration of C–H in methyl group [28], respectively [Fig. 16B(b)]. In addition to the generation of –OH, C=O and –CH₃ groups, a broad featureless shoulder is observed in the range 2,910–2,990 cm⁻¹, due to aliphatic C–H stretching in methylene and methyl groups.

Ar activation of Conc. HNO₃ treated calgon carbon induces certain specific changes into the spectral features. The first and foremost change is the appearance of a broad shoulder at 1,753 cm⁻¹ attributable to the C=O group of carboxylic acid groups Fig. 16B(c). Also, the broad featureless shoulder present in the HNO₃ treated calgon carbon (in the range 2,910–2,990 cm⁻¹) develops into two clear sharp peaks centered at 2,956 and 2,918 cm⁻¹, which are attributed to the asymmetric and symmetric stretching vibrations of C–H in methylene groups indicating the generation of hydrophobic methylene C–H groups on the surface of calgon carbon on activation with Ar. In spite of the several striking changes brought about, as discussed above, into the surface functionality of calgon carbon upon treatment with conc. HNO₃ and subsequent Ar activation, some inherent functional groups of parent calgon carbon remained unaltered even after modification. The spectral features common to all the three samples [Fig. 16B(a–c)] are as follows: a broad intense transmission peak centered at 3,450 cm⁻¹ corresponding to OH stretching mode of hydroxyl groups and adsorbed water and a broad intense peak centered at 1,075 cm⁻¹, which can be attributed to C–O stretching in acids, alcohols, phenols, ethers and esters [52].

13.4 Evaluation the Adsorptive Desulphurization Potential of Adsorbent and Calgon Based Carbon Materials

The results of the adsorptive desulphurization experiments are presented in Table 15. Both nitric acid treatment and

subsequent Ar activation enhanced the S adsorption ability of the carbon samples, the Ar activated samples being more active for adsorption. Combination of nitric acid treatment and Ar activation induces suitable surface functionality, polarity (surface hydrophilic and hydrophobic functional groups), phase structure (discussed under XRD) and pore structure into the carbon adsorbents facilitating enhanced adsorption of the organo-sulphur compounds present in the diesel feed stocks.

The nature of the S components present in the product diesel was analyzed using GC-PFPD and the results obtained over 15.0 g sorbent bed using modified adsorbent carbon (A) and calgon carbon (B) are shown in Table 16. It is observed that the most highly refractive compounds (C_2BT and C_2DBT) present in the feed prior to desulphurization process are absent in the product diesel after the adsorption process exemplifying the utility and usefulness of the process in selectively adsorbing the refractory S-compounds that are difficult to desulfurize over conventional hydrotreating catalysts.

The carbon samples after S-adsorption could be regenerated by washing with toluene (500 mL for 100 g spent carbon) at room temperature followed by drying the sorbent bed at 110 °C. The results of the adsorption experiments over neat and solvent regenerated calgon carbon (without modification) are shown in Fig. 17. It is evident from the adsorption plots that the regenerated sorbents performance is on a par with that of the fresh calgon carbon as received. Thus an efficient and environmentally benign regeneration method and a process for the adsorptive desulfurization appear to be feasible based on carbon materials.

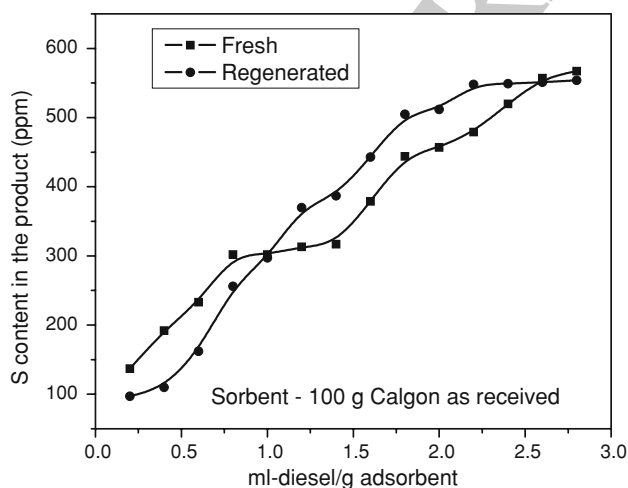


Fig. 17 Plot of S removal capacity of fresh versus toluene regenerated sorbent (100 g calgon carbon used as received)

14 Conclusions

The development of carbon materials has always been a challenging problem from the point of view of their source and activation procedures to create characteristics necessary to exploit them for various applications, including as support for noble metals (used in electrodes and as catalysts for organic transformations) and adsorption purposes. We have reported the use of natural raw materials for developing carbon materials useful in fuel cell electrode applications. We have also demonstrated the use of appropriate activation treatments to modify the textural and surface functionalities at the surface of carbon materials. The possibility of employing these developed carbon materials or carbon materials available from other sources in some applications as supports for electro-catalysts and for specific applications like adsorptive desulfurization has been investigated.

Acknowledgments The authors wish to record their gratefulness to the Department of Science and Technology, India, The Chennai Petroleum Corporation Limited (CPCL) and Ms. Columbian Chemicals Company, USA, for supporting the work.

References

1. Viswanathan B, Indra Neel P, Varadarajan T K (2009) Methods of activation and specific applications of carbon materials, E-book, <http://nccr.iitm.ac.in>
2. Viswanathan B, Aulice Scibioh M (2006) Fuel cells: principles and applications, Universities Press
3. Ren B, Li XQ, She CX, Wu DY, Tian ZQ (2000) *Electrochim Acta* 46:193
4. Carabineiro SAC, David Thompson T (2007) Catalytic applications of gold nanotechnology in nanoscience and technology, nanocatalysis. In: Heiz U, Landman U (eds) Springer, Berlin, p 463
5. Andrew Dicks L (2006) *J Power Sources* 156:128
6. Rajesh B (2002) Methanol oxidation anodes based on conducting polymers and carbon nanotubes supported noble metal (s) for possible applications in DMFC, Ph. D. thesis, Indian Institute of Technology Madras
7. Samant PV, Rangel CM, Romero MH, Fernandes JB, Figueiredo JL (2005) *J Power Sources* 151:79
8. Viswanathan B (2009) *Catal Today* 141:52
9. Mohindar Seehra S, Arthur Pavlovic S (1993) *Carbon* 31:557
10. Suresh Babu V, Seehra MS (1996) *Carbon* 34:1259
11. West AR (1984) *Solid State Chemistry and its Applications*. Wiley, Chichester, p 734
12. Liu Z, Ling XY, Su X, Lee JY (2004) *J Phys Chem B* 108:8234
13. Manohara R, Goodenough JB (1992) *J Mater Chem* 2:875
14. Liu Z, Lee JY, Chen W, Han M, Gan LM (2004) *Langmuir* 20:181
15. Sevilla M, Sanches C, Valdos-Sols T, Moralln E, Fuertes AB (2007) *J Phys Chem C* 111:9749
16. Niu JJ, Wang JN, Zhang L, Shi Y (2007) *J Phys Chem C* 111:10329
17. Lei Z, Bai S, Xiao Y, Dang L, Au L, Zhang G, Xu Q (2008) *J Phys Chem C* 111:722

- 1139 18. Zheng S-F, Hu J-s, Zhong LS, Wan LJ, Song WG (2007) *J Phys Chem C* 111:11174 1174
 1140 19. Sobkowski J, Franaszczuk K, Dobrowolska K (1992) *J Electroanal Chem* 330:529 1175
 1141 20. Wu G, Xu B-Q (2007) *J Power Sources* 174:148 1176
 1142 21. Liu Z, Lee JY, Chen W, Han M, Gan LM (2004) *Langmuir* 20:181 1177
 1143 22. Lin M-L, Huang C-C, Lo M-Y, Mou C-Y (2008) *J Phys Chem C* 112:867 1178
 1144 23. Indra Neel P (2009) *Methods of activation and specific applications of carbon materials from natural sources*, Ph. D. thesis, Indian Institute of Technology Madras 1179
 1145 24. Prahas Devarly, Kartika Y, Indraswati N, Ismadji S (2008) *Chem Eng J* 140:32 1180
 1146 25. Pol VG, Motiei M, Gedanken A, Calderon-Moreno J, Yoshimura M (2004) *Carbon* 42:111 1181
 1147 26. Ruland W (1990) *Adv Mater* 2:528 1182
 1148 27. Ruland W, Smarsly B (2002) *J Appl Crystallogr* 35:624 1183
 1149 28. Yang T, Lua AC (2006) *Mater Chem Phys* 100:438 1184
 1150 29. Lespade P, Al-Jishi R, Dresselhaus MS (1982) *Carbon* 20:427 1185
 1151 30. Rials TG, Glasser WG (1989) *J Appl Polym Sci* 37:2399 1186
 1152 31. Sarkar S, Adhikari B (2001) *Eur Polym J* 37:1391 1187
 1153 32. Kubo S, Uraki Y, Sano Y (2003) *J Wood Sci* 49:188 1188
 1154 33. Sricharoenchaikul V, Pechyen C, Aht-ong D, Atong D (2008) *Energy Fuels* 22:31 1189
 1155 34. Cotton FA, Wilkinson G (1976) *Basic inorganic chemistry*. Wiley, New York 1190
 1156 35. Adams MD (1991) *Hydrometallurgy* 26:201 1191
 1157 36. Sarathi R, Rajesh Kumar P, Sahu RH (2007) *Polym Degrad Stab* 92:560 1192
 1158 37. Manivannan A, Chirila M, Giles NC, Seehra MC (1999) *Carbon* 37:1741 1193
 1159 38. Singer LS, Wagoner G (1968) *Carbon* 6:199 1194
 1160 39. Chauvert O, Forro L (1995) *Phys Rev B Condens Mater* 52:R6963 1195
 1161 40. Zhuo O, Fleming RM, Murphy DW, Chen CH, Haddon RC, Ramirez AP, Gharum SH (1994) *Science* 263:1744 1196
 1162 41. Mrozowski S (1979) *Carbon* 17:227 1197
 1163 42. Freitas JCC, Bonagamba J, Emmerich FG (2001) *Carbon* 39:535 1198
 1164 43. Donnet JB, Bansal R, Wang M-J (1993) *Carbon black—science and technology*, 2nd edn. Revised and expanded. CRC publications 1199
 1165 44. Joong Noh S, James Schwarz A (1990) *Carbon* 28:675 1200
 1166 45. Gomez-Serrano V, Acedo-Ramos M, Lopez-Peinado AJ, Valenzuela-Calahorra C (1997) *Thermochim Acta* 291:109 1201
 1167 46. Shao M, Wang D, Yu G, Hu B, Yu W, Qian Y (2004) *Carbon* 42:183 1202
 1168 47. Macia-Agullo JA, Moore BC, Cazorla-Amoros D, Linares-Solana A (2007) *Microporous Mater* 101:397 1203
 1169 48. Budinova T, Ekinci E, Yardim F, Grimm A, Bjornbom E, Minkova V, Goranova M (2006) *Fuel Process Technol* 87:899 1204
 1170 49. Ishizaki C, Marti I (1981) *Carbon* 19:409 1205
 1171 50. Madhava Rao M, Ramesh A, Purna Chandra Rao G, Seshaiiah K (2006) *J Hazard Mater B* 129:123 1206
 1172 51. Puziy AM, Poddubnaya OI, Martinez-Alonso A, Suarez-Garcia F, Tascon JMD (2003) *Carbon* 41:1181
 1173 52. Alexander Puziy AM, Olga Poddubnaya I, Alonso AM, Garcia FS, Jaun Tascon MD (2005) *Carbon* 43:2857
 53. Gercel O, Ozcan A, Safa Ozcan A, Ferdi Gercel H (2007) *Appl Surf Sci* 253:4843
 54. Macias-Garcia A, Diaz-Diez MA, Cuerda-Correa EM, Olivares-Marin M, Ganan-Gomez J (2006) *Appl Surf Sci* 252:5972
 55. Selvavathi V, Meenakshisundaram A, Sairam B, Indra Neel P, Rajasekaran M, Viswanathan B (2008) *Adsorptive desulphurization of diesel by modified carbons*. In: 6th international symposium on fuels and lubricants (ISFL-2008), March 9–12, 2008 at New Delhi

UNCORRECTED